

BoMb-OT: On Batch of Mini-batches Optimal Transport

Khai Nguyen[◊] Quoc Nguyen[◊] Nhat Ho[†] Tung Pham[◊] Hung Bui[◊]
Dinh Phung[‡] Trung Le[‡]

VinAI Research, Vietnam[◊]; University of Texas, Austin[†]; Monash University[‡]
October 19, 2021

Abstract

Mini-batch optimal transport (m-OT) has been successfully used in practical applications that involve probability measures with intractable density, or probability measures with a very high number of supports. The m-OT solves several sparser optimal transport problems and then returns the average of their costs and transportation plans. Despite its scalability advantage, m-OT is not a proper metric between probability measures since it does not satisfy the identity property. To address this problem, we propose a novel mini-batching scheme for optimal transport, named *Batch of Mini-batches Optimal Transport* (BoMb-OT), that can be formulated as a well-defined distance on the space of probability measures. Furthermore, we show that the m-OT is a limit of the entropic regularized version of the proposed BoMb-OT when the regularized parameter goes to infinity. We carry out extensive experiments to show that the new mini-batching scheme can estimate a better transportation plan between two original measures than m-OT. It leads to a favorable performance of BoMb-OT in the matching and color transfer tasks. Furthermore, we observe that BoMb-OT also provides a better objective loss than m-OT for doing approximate Bayesian computation, estimating parameters of interest in parametric generative models, and learning non-parametric generative models with gradient flow.

1 Introduction

Optimal transport (OT) [65, 66, 56] has emerged as an efficient tool in working with probability measures. Under the name of Wasserstein distance, OT has been widely utilized to solve problems such as generative modeling [2, 63, 58, 29, 44], barycenter problem [32, 39], and approximate Bayesian computation [6, 47]. Furthermore, OT also provides a principle to find the most economical map of moving masses between probability measures, which is very useful in various tasks such as color transfer [26, 54], domain adaptation (alignment) [17], and graph processing [62, 67, 14].

Although OT has attracted growing attention in recent years, a major barrier that prevents OT from being ubiquitous is its heavy computational cost. When the two probability measures are discrete with n supports, solving the Wasserstein distance via the interior point methods has the complexity of $\mathcal{O}(n^3 \log n)$ [53], which is extremely expensive when n is large. There are two main lines of works that focus on easing this computational burden when applying the Wasserstein distance. The first approach is to find a good enough approximation of the solution by adding an entropic regularized term on the objective function [18]. Several works [1, 41] demonstrated that the entropic approach can produce a ε -approximated solution at the same time reduce the computational complexity to $\mathcal{O}(n^2/\varepsilon^2)$. The second line of works named the "slicing" approach, is based on the closed-form of Wasserstein distance in one-dimensional space. There are various variants on this directions; for example [11, 13, 20, 35, 49, 50, 15]. They are all in the family of sliced Wasserstein distances with the computational complexity $\mathcal{O}(n \log n)$. Recently, some methods are proposed to

combine the dimensional reduction approach with the entropic solver of Wasserstein distance to inherit advantages from both directions [52, 46, 40, 42].

Despite the fact that discussed works have reduced the computational cost of OT considerably, computing OT is still challenging in the big data settings where n could be as large as few millions. This situation leads to the development of mini-batch’s method for OT [29, 60], which we refer to as mini-batch OT loss. The main idea of the mini-batch method is to treat each mini-batch as a sample point in product space, then the overall loss is defined as the average of distances between mini-batches. Due to the low computation cost on mini-batch, this scheme was applied for many forms of Wasserstein distances [21, 8, 36, 58], and was theoretically studied in the works of [4, 7, 48]. Recently, [24, 25] formulated this approach by giving an explicit definition of mini-batch OT loss, studying its asymptotic behavior, and investigating its gradient estimation properties. On the other hand, the mini-batch OT loss does not preserve the metricity of optimal transport distances, namely, this loss is always positive even when two probability measures are identical. Furthermore, it is also unclear whether this loss achieves the minimum value when the two probability measures are equal. Because of these issues of mini-batch OT loss, using this loss for applications involving estimating an unknown probability distribution may not lead to desirable estimation.

Contribution. In this paper, we propose a novel mini-batching scheme for optimal transport, which is named as *Batch of Mini-batches Optimal Transport* (BoMb-OT). Instead of using the average of OT costs between mini-batches as a discrepancy, BoMb-OT loss considers each mini-batch as a single point in the product space. Then, the BoMb-OT cost is constructed via a Kantorovich formulation between the product measures of two original measures with the ground cost being a predefined optimal transport cost between mini-batch empirical measures. In summary, our main contributions are two-fold:

1. First, we show that the batch of mini-batches optimal transport is a well-defined metric on the space of probability measures. Furthermore, the entropic regularization version of BoMb-OT, which we refer to as entropic BoMb-OT (eBoMb-OT), admits the traditional m-OT as the special case, namely, when the regularization parameter in the eBoMb-OT goes to infinity, the value of eBoMb-OT approaches the value of m-OT. Finally, due to the intractable computation of BoMb-OT when the two probability measures are continuous, we propose the empirical and sub-sampling versions of BoMb-OT. Given the discrete versions, we also propose the algorithm to obtain the transportation plan between the original measures from BoMb-OT in both the hypothetical case and the sub-sampling case.
2. Second, we demonstrate the favorable performance of BoMb-OT over m-OT in various applications, such as sample matching, approximate Bayesian computation, color transfer, generative adversarial network, and gradient flow. In these applications, we also provide a careful investigation of the effects of two hyper-parameters of the mini-batching scheme, which are the number of mini-batches and the size of mini-batches, on the performance of BoMb-OT and m-OT.

Organization: The remainder of the paper is organized as follows. In Section 2, we provide backgrounds for optimal transport distances and the conventional mini-batching scheme (m-OT). In Section 3, we define the new mini-batching scheme for optimal transport distances, Batch of mini-batches Optimal Transport, and derive some of its theoretical properties. Section 4 benchmarks the proposed mini-batch scheme by extensive experiments on large-scale datasets, and followed by

discussions in Section 5. Finally, proofs of key results and extra materials are in the supplementary material.

Notation: For any probability measure μ on the Polish measurable space (\mathcal{X}, Σ) , we denote $\mu^{\otimes m}$ ($m \geq 2$) as the product measure $\underbrace{\mu \times \dots \times \mu}_m$ on the product measurable space $(\mathcal{X}^m, \Sigma^m)$, where

$\mathcal{X}^m := \underbrace{\mathcal{X} \times \dots \times \mathcal{X}}_m$ and $\Sigma^m := \underbrace{\Sigma \otimes \dots \otimes \Sigma}_m$. For any $p \geq 1$, we define $\mathcal{P}_p(\mathbb{R}^N)$ as the set of Borel

probability measures with finite p -th moment defined on a given metric space $(\mathbb{R}^N, \|\cdot\|)$. For any random vector $X^m = (x_1, \dots, x_m) \in \mathcal{X}^m$, we define by $P_{X^m} := \frac{1}{m} \sum_{i=1}^m \delta_{x_i}$ the empirical measures associated with X^m . For any set $\{x_1, \dots, x_n\}$ and $m \geq 1$, we denote by $[\{x_1, \dots, x_n\}]^m$ the set of all subsets with m elements of $\{x_1, \dots, x_n\}$. For any joints probabilities γ and π in $\mathcal{X}^m \times \mathcal{X}^m$, the relative entropy between π and γ is defined as follows:

$$H(\gamma|\pi) := \int_{\mathcal{X}^m \times \mathcal{X}^m} \log \left(\frac{d\gamma}{d\pi}(x, y) \right) d\gamma(x, y),$$

where $\frac{d\gamma}{d\pi}(x, y)$ denotes the density of γ with respect to π .

2 Background

In this section, we review the definitions of Wasserstein distance, entropic Wasserstein, and sliced Wasserstein distance. Then, we recall the definition of mini-batch optimal transport that has been widely used in applications.

2.1 Wasserstein distance and its variants

We first start with the definition of Wasserstein distance. Assume that μ and ν are two probability measures on $\mathcal{P}_p(\mathbb{R}^N)$. The Wasserstein distance between μ and ν is defined as follows:

$$W_p(\mu, \nu) := \left[\min_{\pi \in \Pi(\mu, \nu)} \mathbb{E}_{\pi(x, y)} \|x - y\|^p \right]^{\frac{1}{p}},$$

where $\Pi(\mu, \nu) := \{\pi : \int \pi dx = \nu, \int \pi dy = \mu\}$ is the set of transportation plans between μ and ν .

Entropic regularized Wasserstein: The entropic regularized Wasserstein to approximate the OT solution [1, 41] between μ and ν is defined as follow [18]:

$$W_p^\tau(\mu, \nu) := \min_{\pi \in \Pi(\mu, \nu)} \left[\mathbb{E}_{\pi(x, y)} \|x_i - y_j\|^p \right]^{\frac{1}{p}} + \tau H(\pi | \mu \otimes \nu),$$

where $\tau > 0$ is a chosen regularized parameter.

Sliced Wasserstein distance: Sliced Wasserstein (SW) [12, 11] is motivated by the closed-form of the Wasserstein distance in one dimensional space. Based on that formula, SW is defined as the average of all Wasserstein distances between one-dimensional probability measures that are obtained

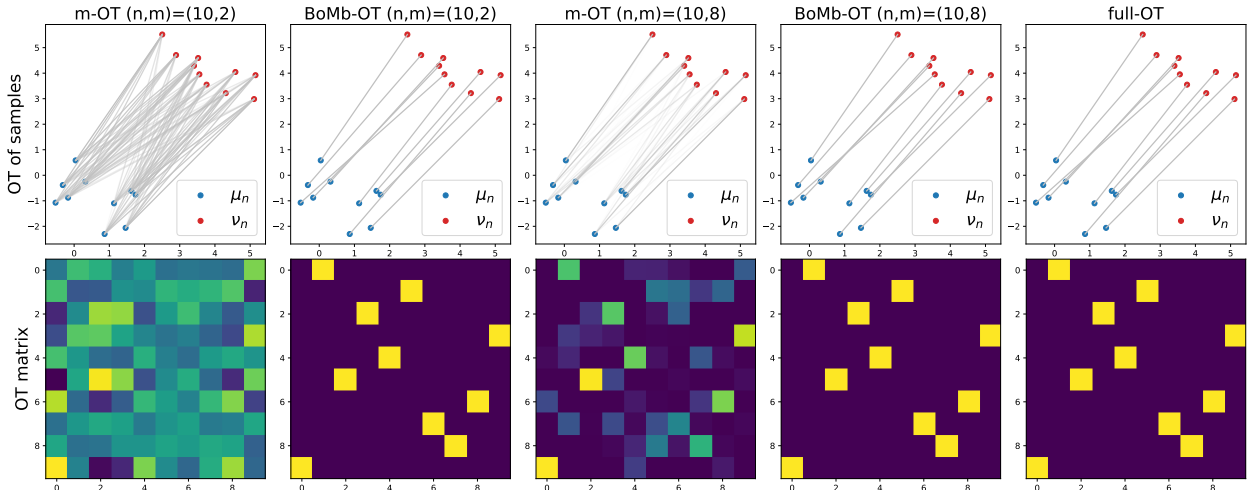


Figure 1: The first row provides a visualization of transportation between two 2D empirical distributions with 10 samples from m-OT, BoMb-OT, and full OT approach. The next row is the corresponding optimal plan matrices.

by orthogonally projecting two original measures into one-dimensional spaces. The formal definition of SW is:

$$SW_p(\mu, \nu) := \left[\mathbb{E}_{\theta \sim \mathcal{U}(\mathbb{S}^{N-1})} W_p^p(\theta \sharp \mu, \theta \sharp \nu) \right]^{\frac{1}{p}},$$

where $\mathcal{U}(\mathbb{S}^{N-1})$ denotes the uniform measure over the d -dimensional unit hypersphere, $\theta \sharp$ is the orthogonal projection operator on direction θ . Due to the intractability of the expectation, SW is usually approximated by its empirical version using direction $\theta_{1:L}$ where $\theta_{1:L}$ are L unit vectors generated from $\mathcal{U}(\mathbb{S}^{N-1})$. When μ and ν are discrete probability measures with at most n supports, the complexity of computing SW is at the order of $\mathcal{O}(Ln \log n)$.

2.2 Mini-batch Optimal Transport

In this section, we revisit the definition of mini-batch OT loss in [24] (cf. Definition 1 in that work). Note that, some of the notations in that definition are adapted to this paper.

Definition 1. Assume that μ and ν are two probability measures on $\mathcal{P}_p(\mathcal{X})$ for some given $p \geq 1$. For $m \geq 1$, let $d : \mathcal{P}_p(\mathcal{X}) \times \mathcal{P}_p(\mathcal{X}) \rightarrow [0, \infty)$ be a given function. Then, the mini-batch OT (m-OT) loss between μ and ν is defined as follows:

$$U_d(\mu, \nu) := \mathbb{E}_{(X^m, Y^m) \sim \mu^{\otimes m} \otimes \nu^{\otimes m}} d(P_{X^m}, P_{Y^m}). \quad (1)$$

Due to the intractability of the outer expectation in equation (1), [24] consider both the discrete-discrete loss and mini-batch subsampling loss versions of the mini-batch OT (see Definitions 8 and 9 in Appendix B for more details). We also review the definitions of transportation plan and sub-sampling transportation plan of m-OT (cf. Definition 3 in [24]) in Definition 10 and Definition 11 in Appendix B.

Properties of the mini-batch OT loss: By Proposition 3 in [24], the mini-batch OT loss is symmetric and positive, but it does not equal 0 when the measure μ and ν are equal. Furthermore, it is also unclear whether the loss attains its minimum value when μ and ν are identical. That aspect of m-OT can be undesirable for using to estimate unknown probability distributions.

3 Batch of Mini-batches Optimal Transport

In order to address the issue of m-OT, in this section, we first propose a novel mini-batch loss, named batch of mini-batches OT (BoMb-OT) loss, between continuous probability measures. We show that this loss is a well-defined metric in the space of Borel probability measures. Then, we propose empirical versions of BoMb-OT to account for the computational intractability of BoMb-OT. Finally, we show how to combine the transport plans of BoMb-OT and the transport plans between mini-batches to estimate the transportation plan for the whole data set.

In order to simplify the presentation in this section, we assume throughout this section that μ and ν are continuous probability measures in $\mathcal{P}_p(\mathcal{X})$ for some given $p \geq 1$ and $\mathcal{X} \subset \mathbb{R}^N$ where $N \geq 1$. Furthermore, $d : \mathcal{P}_p(\mathcal{X}) \times \mathcal{P}_p(\mathcal{X}) \rightarrow [0, \infty)$ is a given divergence between probability measures in $\mathcal{P}_p(\mathcal{X})$.

3.1 Definition and Metricity

We first start with the following definition of the batch of mini-batches OT loss between probability measures.

Definition 2. *The Batch of Mini-batches OT (BoMb-OT) loss between probability measures μ and ν is defined as:*

$$\mathcal{D}(\mu, \nu) := \inf_{\gamma \in \Pi(\mu^{\otimes m}, \nu^{\otimes m})} \mathbb{E}_{(X^m, Y^m) \sim \gamma} [d(P_{X^m}, P_{Y^m})].$$

Instead of taking the average of distances between all pairs of mini-batches as in Definition 1, here we find the optimal plan between two distributions on mini-batches. This property is crucial to guarantee that BoMb-OT loss equals zero when $\mu \equiv \nu$ and hence is a well-defined metric in the space of probability measures.

Theorem 1. *Assume that d is an invariant metric under permutation on \mathcal{X}^m and the function $d(P_{x^m}, P_{y^m})$ is continuous in terms of $x^m, y^m \in \mathcal{X}^m$. Then, BoMb-OT is a well-defined metric in the space of probability measures.*

The proof of Theorem 1 is in Appendix A. The assumption of Theorem 1 is mild and satisfied when d is (sliced) Wasserstein metric of order p , i.e., $d \in \{W_p, SW_p\}$.

Entropic regularization version of BoMb-OT and its connection to m-OT: We now consider an entropic regularization of BoMb-OT, which is particularly useful for reducing the computational complexity of BoMb-OT. In particular, the *entropic regularized BoMb-OT* (eBoMb-OT) between two probability measures μ and ν admits the following form:

$$\mathcal{ED}(\mu, \nu) := \inf_{\gamma \in \Pi(\mu^{\otimes m}, \nu^{\otimes m})} \mathbb{E}_{(X^m, Y^m) \sim \gamma} [d(P_{X^m}, P_{Y^m})] + \lambda \text{H}(\gamma | \mu^{\otimes m} \otimes \nu^{\otimes m}), \quad (2)$$

where $\lambda > 0$ stands for a chosen regularized parameter. Definition 2 is an interpolation between BoMb-OT and m-OT. On one hand, when $\lambda \rightarrow 0$, it is known that $\mathcal{ED}(\mu, \nu)$ converges to $\mathcal{D}(\mu, \nu)$. On the other hand, when $\lambda \rightarrow \infty$, the joint distribution γ equals $\mu^{\otimes m} \otimes \nu^{\otimes m}$, then $\mathcal{ED}(\mu, \nu)$ converges to $U_d(\mu, \nu)$.

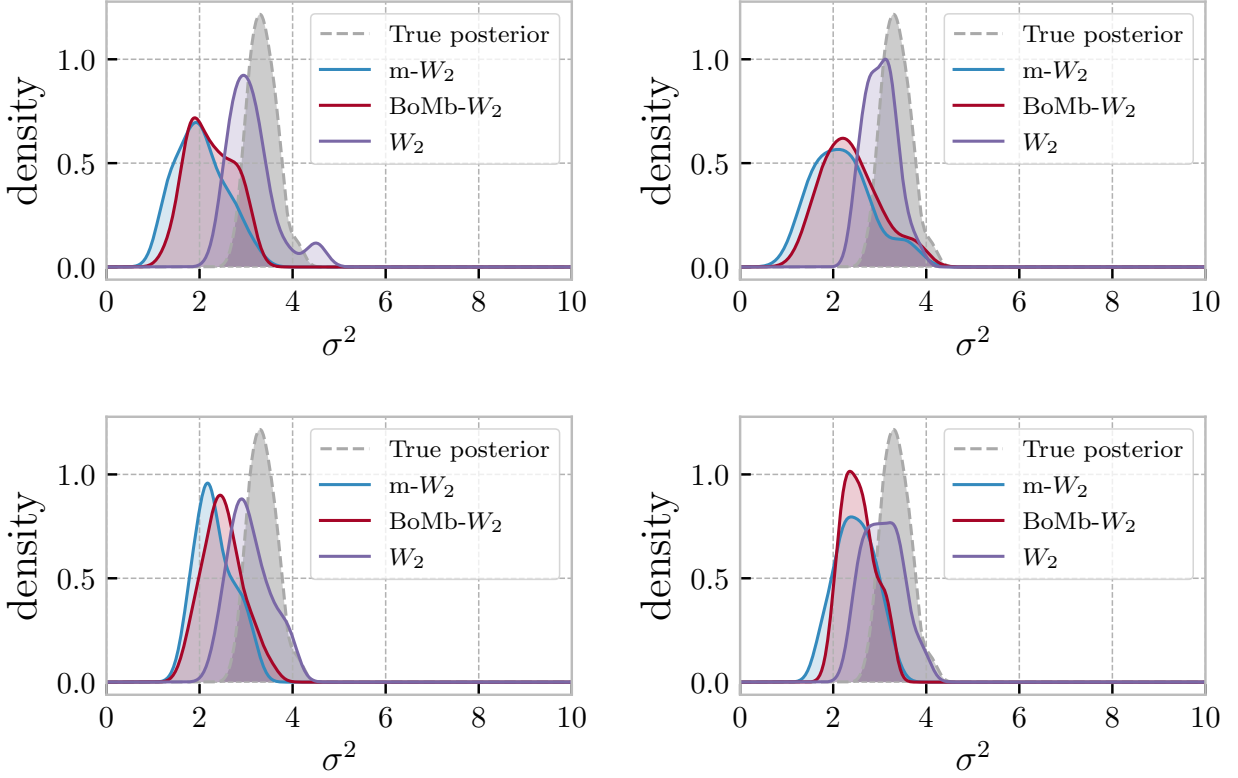


Figure 2: Approximated posteriors from ABC with different losses. Here, the number of mini-batches 2, 4 in the first row and 8, 16 in the second row, batch size $m = 32$, and the dimension equals 2.

3.2 Empirical versions of BoMb-OT

Similar to the mini-batch OT loss, the formula of the BoMb-OT loss is intractable. Therefore, we will consider empirical versions of BoMb-OT to approximate the value of BoMb-OT. A natural way is to define the empirical BoMb-OT on empirical distributions of $\mu^{\otimes m}$ and $\nu^{\otimes m}$ as follows:

Definition 3. Assume that $X_1^m, \dots, X_k^m \stackrel{i.i.d.}{\sim} \mu^{\otimes m}$ and $Y_1^m, \dots, Y_k^m \stackrel{i.i.d.}{\sim} \nu^{\otimes m}$ where $k \geq 1$ is given. We denote $\mu_k^{\otimes m} := \frac{1}{k} \sum_{i=1}^k \delta_{X_i^m}$ and $\nu_k^{\otimes m} := \frac{1}{k} \sum_{i=1}^k \delta_{Y_i^m}$. Then, the empirical BoMb-OT loss between μ and ν is defined as follows:

$$\tilde{D}_k(\mu, \nu) := \min_{\gamma \in \Pi(\mu_k^{\otimes m}, \nu_k^{\otimes m})} \mathbb{E}_{(X^m, Y^m) \sim \gamma} [d(P_{X^m}, P_{Y^m})].$$

Computational complexity: The computational complexity of $\tilde{D}_k(\mu, \nu)$ depends on a particular choice of d . For the experiments in the paper, we specifically consider three choices of $d \in \{W_p, W_p^r, S_p\}$. Here, we only discuss the case when $d = W_p$ (The discussion with other choices of d is in Appendix B). When d is Wasserstein distance, for each pair X_i^m and Y_i^m , the computational complexity of approximating $d(P_{X_i^m}, P_{Y_i^m})$ via the Sinkhorn algorithm is of order $\mathcal{O}(m^2/\varepsilon^2)$ where $\varepsilon > 0$ is some desired accuracy [41]. It suggests that the complexity of computing the cost matrix from the empirical BoMb-OT is of order $\mathcal{O}(k^2 m^2 / \varepsilon^2)$. Given the cost matrix, the empirical BoMb-OT can be approximately computed via Sinkhorn algorithm with the complexity of the order $\mathcal{O}(k^2 / \varepsilon^2)$. Therefore, the total computational complexity of computing the empirical BoMb-OT is $\mathcal{O}(k^2 m^2 / \varepsilon^2)$.

Sample complexity: The next thing that we want to guarantee is the approximation error between the empirical BoMb-OT and BoMb-OT. We first provide the following result with the approximation error when $d \equiv W_p$.

Theorem 2. *Assume that $d \equiv W_p$ for some $p \geq 1$ and \mathcal{X} is a compact subset of \mathbb{R}^N . Then, the following holds:*

$$|\tilde{\mathcal{D}}_k(\mu, \nu) - \mathcal{D}(\mu, \nu)| = \mathcal{O}_P\left(\frac{m^{1-1/p}}{k^{1/N}}\right).$$

The proof of Theorem 2 is in Appendix A. We would like to remark that the dependency of the sample complexity of empirical BoMb-OT on N is necessary when $d \equiv W_p$. It is due to the inclusion of the additional optimal transport in BoMb-OT. One way to deal with the curse of dimensionality of empirical BoMb-OT is to choose $d \equiv SW_p$ where we prove in Appendix B that the approximation error under this case is at the order $\mathcal{O}_P(m^{1-1/p}/\sqrt{k})$. Note that, this choice $d \equiv SW_p$ improves not only the sample complexity but also the computational complexity of empirical BoMb-OT. In particular, in Appendix B, we demonstrate that the computational complexity of empirical BoMb-OT is $\mathcal{O}(k^2 m \log m)$ when $d \equiv SW_p$. Another potential way to deal with the curse of dimensionality of empirical BoMb-OT is to use its entropic version. The entropic optimal transport had been shown to have sample complexity at the order $k^{-1/2}$ [45]. In the case of entropic empirical BoMb-OT, when the regularized parameter is infinity, namely, m-OT, the result of [24, 25] already established the sample complexity $k^{-1/2}$. However, for a general value of the regularized parameter, it is unclear whether we still have this sample complexity $k^{-1/2}$ of the entropic regularized BoMb-OT. We leave this question for future work.

Mini-batch contexts: In practice, we are given $X^n := x_1, \dots, x_n$ i.i.d. samples from the distribution μ and $Y^n := y_1, \dots, y_n$ i.i.d. samples from the distribution ν . Let $\mu_n = \frac{1}{n} \sum_{i=1}^n \delta x_i$ and $\nu_n = \frac{1}{n} \sum_{i=1}^n \delta y_i$ be two corresponding empirical measures, we further define $\mu_n^{\otimes m}$ and $\nu_n^{\otimes m}$:

$$\mu_n^{\otimes m} := \frac{1}{\binom{n}{m}} \sum_{X_i^m \in \binom{X^n}{m}} \delta_{X_i^m}, \quad \nu_n^{\otimes m} := \frac{1}{\binom{n}{m}} \sum_{Y_j^m \in \binom{Y^n}{m}} \delta_{Y_j^m},$$

where $\binom{S}{m}$ is the set of all m -subsets of S . Given these notations, the discrete version of BoMb-OT loss, named *discrete BoMb-OT*, takes the following form.

Definition 4. *The discrete BoMb-OT loss between probability measures μ and ν is given by:*

$$\mathcal{D}_m(\mu, \nu) := \min_{\gamma \in \Pi(\mu_n^{\otimes m}, \nu_n^{\otimes m})} \sum_{i=1}^{\binom{n}{m}} \sum_{j=1}^{\binom{n}{m}} \gamma_{ij} d(P_{X_i^m}, P_{Y_j^m}).$$

Since n is often a very large number in practice, we consider the sub-sampling version of BoMb-OT loss. Instead of using all $\binom{n}{m}$ sets, this version only uses $k > 0$ sets of m samples. We first define:

$$\mu_k^{\otimes m} := \frac{1}{k} \sum_{i=1}^k \delta_{X_i^m}, \quad \nu_k^{\otimes m} := \frac{1}{k} \sum_{j=1}^k \delta_{Y_j^m}.$$

The sub-sampling BoMb-OT is defined as:

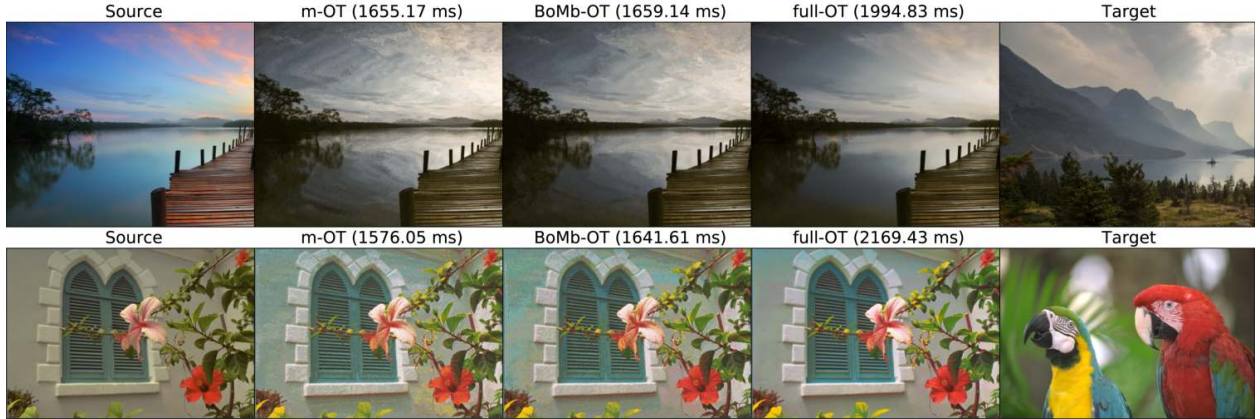


Figure 3: Source images, target images, and transferred images from m-OT, BoMb (the number of mini-batches $k = 60$, the mini-batch's size $m = 50$), full-OT, and corresponding computational times.

Definition 5. *The sub-sampling BoMb-OT loss between probability measures μ and ν is given by:*

$$\mathcal{D}_k(\mu, \nu) := \min_{\gamma \in \Pi(\mu_k^{\otimes m}, \nu_k^{\otimes m})} \sum_{i=1}^k \sum_{j=1}^k \gamma_{ij} d(P_{X_i^m}, P_{Y_j^m}).$$

The computational complexity of sub-sampling BoMb-OT is similar to that of empirical BoMb-OT, which is better than that of discrete BoMb-OT loss. Due to its favorable computation, we will mainly use the sub-sampling BoMb-OT loss in our experiments in Section 4.

Mini-batch transportation plans: We now discuss methods to obtain the transportation plan in mini-batch contexts with BoMb-OT. Recall that, μ_n and ν_n are two empirical measures. We first start with the definition of transportation plan with respect to the discrete BoMb-OT, which is stated as follows. We denote a few notations for the definition. For each $X_i^m \in \binom{X^n}{m}$ and $Y_j^m \in \binom{Y^n}{m}$, we denote by $\pi_{X_i^m, Y_j^m}$ the transportation plan between $P_{X_i^m}$ and $P_{Y_j^m}$ such that $\pi_{X_i^m, Y_j^m}$ is a $n \times n$ matrix where all entries equal zero except those indexed of samples in $X_i^m \times Y_j^m$. Furthermore, the optimal transportation plan γ in discrete BoMb-OT loss in Definition 4 is a $\binom{n}{m} \times \binom{n}{m}$ matrix which is obtained by solving the optimal transport problem between $\mu_n^{\otimes m}$ and $\nu_n^{\otimes m}$.

Definition 6. *The discrete BoMb-OT's transportation plan is given by:*

$$\pi_m(\mu_n, \nu_n) := \sum_{i=1}^{\binom{n}{m}} \sum_{j=1}^{\binom{n}{m}} \gamma_{ij} \pi_{X_i^m, Y_j^m}. \quad (3)$$

Since $\binom{n}{m}$ is often very large, we consider the sub-sampling BoMb-OT's transportation plan. In particular, we only take $k > 0$ sets from each $\binom{X^n}{m}$ and $\binom{Y^n}{m}$. Then, the sub-sampling BoMb-OT's transportation plan is defined as:

Definition 7. *Let k be a positive integer, $X_1^m, \dots, X_k^m \in \binom{X^n}{m}$ and $Y_1^m, \dots, Y_k^m \in \binom{Y^n}{m}$. Denote γ a $k \times k$ optimal transport matrix between $\mu_k^{\otimes m}$ and $\nu_k^{\otimes m}$ in the sub-sampling BoMb-OT loss. Then, the sub-sampling BoMb-OT's transportation plan is defined as:*

$$\pi_k(\mu_n, \nu_n) := \sum_{i=1}^k \sum_{j=1}^k \gamma_{ij} \pi_{X_i^m, Y_j^m}. \quad (4)$$

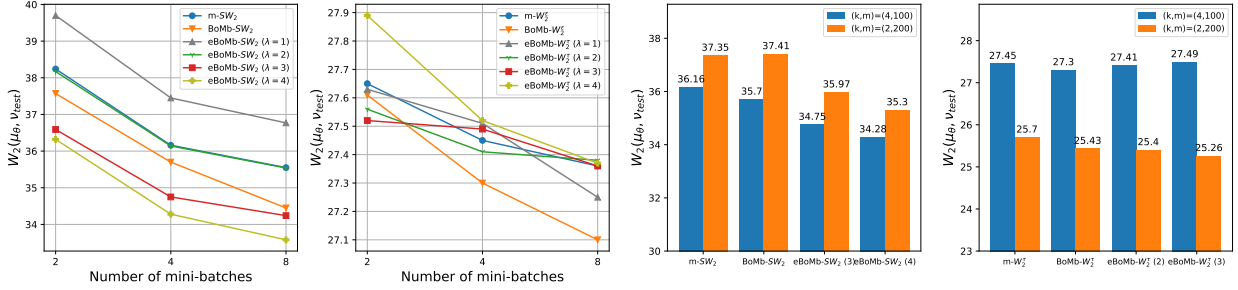


Figure 4: The first two graphs show the changing of the Wasserstein score of mini-batch losses (SW_2 for the first graph and W_2^T for the second graph) when increasing the number of mini-batches ($k \in \{2, 4, 8\}$) on MNIST dataset. The last two graphs are comparing two settings of (k, m) which are $\{(4, 100), (2, 200)\}$.

Intuitively, if optimal transport finds the optimal solution to move products between factories and ports, we can interpret BoMb-OT as hierarchical OT where factories and ports are divided into sub-groups. Then, for each pair of factories-group and ports-group, BoMb-OT computes its optimal transport cost and optimal transportation plan between factories and ports in those sub-groups. After having costs from all pairs, BoMb-OT seeks for the optimal transportation among sub-groups of factories and sub-groups of ports. Finally, BoMb-OT combines it with the OT inside each pair of sub-groups to produce the final cost and the final transportation plan. The pseudo code for sub-sampling BoMb-OT is presented in Algorithm 1 in Appendix B.

4 Experiments

In this section, our first goal is to demonstrate that the BoMb-OT performs better than m-OT in recovering the optimal plan via a toy example on synthetic data. We then compare BoMb-OT and m-OT by applying them to several famous applications of OT, such as approximate Bayesian computation [61, 3], color transfer [57, 26, 54, 10], parametric generative model [30, 29, 21], and gradient flow [55, 59, 44]. The detailed settings including neural network architecture, hyper-parameters, and evaluation metric are in Appendix D. Recall that k is the number of mini-batches and m is the mini-batch size.

4.1 Transportation plans

We present a toy example with 10 blues and 10 red points in Figure 1 to illustrate the transportation plans of m-OT, BoMb-OT, and original OT (full-OT). The optimal transport between them is a one-to-one mapping shown in the last column of Figure 1. The result is identical to the transportation plans produced by the BoMb-OT whenever batch-size is small (2) or larger (8). However, for the m-OT method, we only obtain a chaotic mapping between the two point-clouds when batch-size equals 2. Increasing the size of mini-batches to 8, the obtained map is still noisy, namely, a green point is still mapped to several red points.

The illustration for sub-sampling plans of m-OT and BoMb-OT is given in Figure 6 in Appendix C.1. From these results, we conclude that BoMb-OT’s transportation plan is also better than that of m-OT in sub-sampling cases, namely, BoMb-OT can put masses to correct entries of the transportation matrix while m-OT does not do this job well.

Finally, we show the transportation plans of eBoMb-OT for $\lambda \in \{0.1, 10^3\}$ in Figure 7 in Appendix

C.1 to illustrate its interpolation property. For $\lambda = 10^3$, the eBoMb-OT reverts into m-OT since its sample matching and transportation matrices are the same as those of m-OT. When λ equals 0.1, eBoMb-OT can still provide a sufficiently good solution for the optimal transport problem.

4.2 Approximate Bayesian Computation (ABC)

Due to the efficiency in working with empirical measures, Wasserstein distances are successfully applied to ABC [6, 47]. In this section, we evaluate two mini-batching schemes: m-OT and BoMb-OT on this task by comparing their posterior densities to the true posterior in a conjugate prior setting. The further detail of ABC is described in Appendix C.2. Now, we go straight to the comparison result between m-OT and BoMb-OT in approximating the true posterior.

We use the same setup as in [47]: there are $n = 100$ observations $\{x_i\}_{i=1}^n$ i.i.d from multivariate Gaussian $\mathcal{N}(\mu_*, \sigma_*^2 I_N)$ where N is the dimension, $\mu_* \sim \mathcal{N}(0, I_N)$ and $\sigma_*^2 = 4$. The task is to estimate the posterior of σ^2 under the imaginary assumption that σ^2 follows inverse gamma distribution $\mathcal{IG}(1, 1)$. Under these assumptions, the posterior of σ^2 has the form $\mathcal{IG}(1+n\frac{d}{2}, 1+\frac{1}{2}\sum_{i=1}^n \|x_i - \nu_*\|^2)$. For ABC, we use Wasserstein distance of order 2 and the two mini-batching losses of m-OT and BoMb-OT where the size of mini-batches' size is set to 32, the number of mini-batches is in $\{2, 4, 8, 16\}$ for the acceptance-rejection sampling's criteria in sequential Monte Carlo ABC [64] (using implementation from pyABC [34] with 100 particles and 10 iterations). After obtaining all samples, we estimate their densities by utilizing Gaussian kernel density estimation and then plot the approximated posteriors and the true posterior in Figure 2. It is obvious that the approximated posteriors by BoMb-OT are closer to the true posterior and Wasserstein's posteriors than that of m-OT with every value of the number of mini-batches. In addition, we also show the results for various pairs (k, m) in Figure 8 in Appendix C.1 that further strengthen the claim that BoMb-OT is better than m-OT.

4.3 Color Transfer

As presented in [24], using m-OT helps to make the color transfer framework scalable. In this paper, we focus on another perspective which is the ability to reform the origin transport plan of mini-batching schemes. The details of color transfer and its algorithms are given in Algorithm 3 in Appendix C.3.

A part of the result of the color transfer task is presented in Figure 3 show that BoMb-OT's images are smoother than produced by the m-OT. Moreover, images from BoMb-OT look more identical to the full-OT's transferred images. The reason for this phenomenon is the higher quality of transportation plans of BoMb-OT over m-OT. This claim is reinforced by the additional results in Figure 9 in Appendix C.3. With a very small value of m , m-OT degenerates and achieves very low-quality images while BoMb-OT still can generate almost alike the true images. To show the generalization of the comparison over multiple domains of images, we compare BoMb-OT and m-OT on painting images in Figure 10 in Appendix C.3 where BoMb-OT also shows its favorable performance. In addition, we show by experiment that eBoMb-OT turns to m-OT when the regularized parameter $\lambda \rightarrow \infty$, we set a large value for λ , namely $\lambda = 10^9$, then we show the transferred images in Figure 11 in Appendix C.3. From the computational aspect, BoMb-OT is faster than the original OT when the number of mini-batches k and the mini-batch's size m is chosen correctly. However, BoMb-OT is slower than m-OT due to the extra optimal transportation problem.

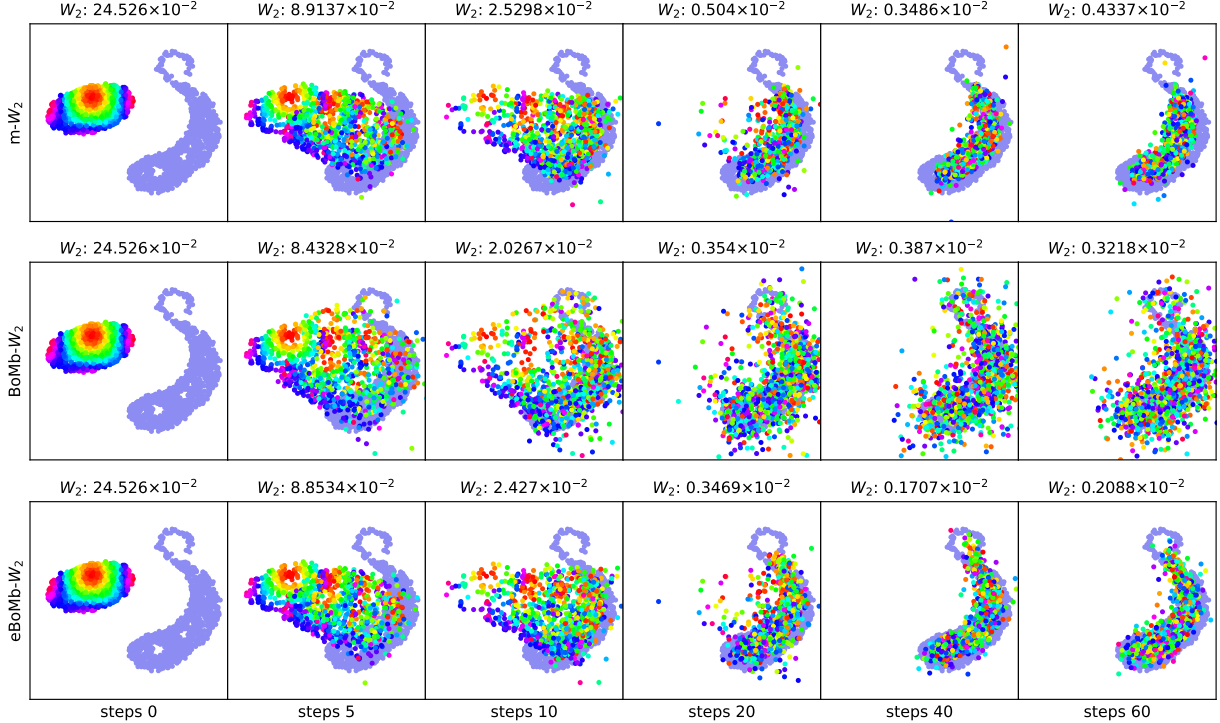


Figure 5: Comparison between (e)BoMb-OT and m-OT in gradient flow with $n = 1000$, $k = 50$, $m = 5$.

Note that, since the reported speed may be affected by the software implementation, we refer the readers to Section 3.2 for the discussion with the computational complexity of BoMb-OT.

4.4 Parametric generative model

In this task, we train generators on MNIST [38], CIFAR10 (64x64) [37], and CelebA (64x64) [43] using different mini-batching schemes with two OT losses: SW_2 and W_2^T (the entropic W_2). On the MNIST dataset, we evaluate the performances of generators by computing Wasserstein-2 scores while we use FID score [31] on CIFAR10 and CelebA. Further detail of this application, all hyperparameter settings, and evaluation metrics are presented in Appendix D.1.

MNIST: We first compare m-OT and BoMb-OT performances with several values of k . In particular, we compute the Wasserstein-2 scores of trained generative models with (SW_2, W_2^T) whose the corresponding scores are recorded in two first graphs in Figure 4. For both divergences, we set $m = 100$, vary $k \in \{2, 4, 8\}$, and train the generative models with 6×10^4 iterations. It is obvious that (e)BoMb-OT’s score curves are always lower than that of m-OT, which means that (e)BoMb-OT helps to learn a better generative model than m-OT with all tested k . It is also apparent that a higher k results in a lower Wasserstein score. Under certain settings, eBoMb-OT performs better than BoMb-OT. This might be due to the effect of the smoother objective function of eBoMb-OT over BoMb-OT [59, 29]. The generated images for qualitative comparison are shown in Figure 14 in Appendix C.4.

In addition, we try to find out what is more important between k and m . In particular, we choose $(k, m) = (4, 100)$ and $(k, m) = (2, 200)$ thus there are totally 400 datum. We run experiments with (SW_2, W_2^T) then report the Wasserstein scores in the last two graphs of Figure 4. For SW_2

distance, it appears that less sample in mini-batch with more mini-batches will produce a better Wasserstein score. However, when using the W_2^r , the opposite happens, a larger sample will result in better performance. A criterion is to choose (k, m) based on the computational analysis of BoMb-OT in Section 3.2 to reduce the running time.

CelebA and CIFAR10: We carry out the same experiments as we did with MNIST. The final result is shown in Figures 12-13 in Appendix C.4. According to these figures, the best generative model is always trained by BoMb-OT or eBoMb-OT. This result is consistent with every choice of (k, m) . However, due to the non-stable metric learning module (L_2 ground metric is not efficient, see Appendix C.4 for the details), we cannot make any conclusion about the effect of the number of mini-batches, namely, the FID curves fluctuate over the x-axis (k) – the number of mini-batches. For qualitative comparison, we illustrate generated images in Figures 15- 16 in Appendix C.4.

4.5 Non-parametric generative model via gradient flow

We also test the performance of BoMb-OT and m-OT in the gradient flow application. We first consider the toy example as in [27] and present our results in Figure 5. The task is to move the colorful empirical measure to the "S-shape" measure. Each measure has 1000 support points. Here, we choose $(k, m) = (50, 5)$, the OT loss is Wasserstein-2, and we use the Wasserstein-2 score to evaluate the performance of the mini-batching scheme. From Figure 5, BoMb-OT and eBoMb-OT provide better flows than m-OT, namely, Wasserstein-2 scores of BoMB-OT and eBoMb-OT are always lower than those of m-OT in every step. Surprisingly, eBoMb-OT achieves the best quality at the end although BoMb-OT is better in the first 10 steps. A possible explanation for this phenomenon is due to the smoothness of loss function, namely, entropic regularization is the smoothing version of original OT, which is only sub-differential [59]. Further detailed description of gradient flow and the experiments on CelebA dataset are deferred to Appendix C.5. Overall, (e)BoMb-OT has better results than m-OT in every setting.

5 Conclusion

In the paper, we have presented a novel mini-batching scheme for optimal transport, named Batch of Mini-batches Optimal Transport (BoMb-OT). The idea of BooMb-OT is to consider the optimal transport problem on the product measure space with a Wasserstein-types ground metric. We prove that BoMb-OT is a valid distance between probability measures and its entropic regularization version, eBoMb-OT, is the generalization of conventional mini-batch optimal transport. More importantly, we have shown that BoMb-OT and eBoMb-OT have more favorable performance than m-OT in various applications of optimal transport.

References

- [1] J. Altschuler, J. Niles-Weed, and P. Rigollet. Near-linear time approximation algorithms for optimal transport via Sinkhorn iteration. In *Advances in neural information processing systems*, pages 1964–1974, 2017. (Cited on pages 1 and 3.)
- [2] M. Arjovsky, S. Chintala, and L. Bottou. Wasserstein generative adversarial networks. In *International Conference on Machine Learning*, pages 214–223, 2017. (Cited on page 1.)

- [3] M. A. Beaumont, W. Zhang, and D. J. Balding. Approximate Bayesian computation in population genetics. *Genetics*, 162(4):2025–2035, 2002. (Cited on pages 9 and 26.)
- [4] M. G. Bellemare, I. Danihelka, W. Dabney, S. Mohamed, B. Lakshminarayanan, S. Hoyer, and R. Munos. The cramer distance as a solution to biased Wasserstein gradients. *arXiv preprint arXiv:1705.10743*, 2017. (Cited on page 2.)
- [5] I. Berkes and W. Philipp. An almost sure invariance principle for the empirical distribution function of mixing random variables. *Zeitschrift für Wahrscheinlichkeitstheorie und verwandte Gebiete*, 41(2):115–137, 1977. (Cited on page 19.)
- [6] E. Bernton, P. E. Jacob, M. Gerber, and C. P. Robert. Approximate Bayesian computation with the Wasserstein distance. *Journal of the Royal Statistical Society*, 2019. (Cited on pages 1, 10, and 26.)
- [7] E. Bernton, P. E. Jacob, M. Gerber, and C. P. Robert. On parameter estimation with the Wasserstein distance. *Information and Inference: A Journal of the IMA*, 8(4):657–676, 2019. (Cited on page 2.)
- [8] B. Bhushan Damodaran, B. Kellenberger, R. Flamary, D. Tuia, and N. Courty. Deepjdot: Deep joint distribution optimal transport for unsupervised domain adaptation. In *Proceedings of the European Conference on Computer Vision (ECCV)*, pages 447–463, 2018. (Cited on page 2.)
- [9] S. Bobkov and M. Ledoux. ‘one-dimensional empirical measures, order statistics, and Kantorovich transport distances. *Memoirs of the American Mathematical Society*, 261, 2019. (Cited on page 20.)
- [10] N. Bonneel and D. Coeurjolly. Spot: sliced partial optimal transport. *ACM Transactions on Graphics (TOG)*, 38(4):1–13, 2019. (Cited on page 9.)
- [11] N. Bonneel, J. Rabin, G. Peyré, and H. Pfister. Sliced and Radon Wasserstein barycenters of measures. *Journal of Mathematical Imaging and Vision*, 1(51):22–45, 2015. (Cited on pages 1 and 3.)
- [12] N. Bonnotte. *Unidimensional and evolution methods for optimal transportation*. PhD thesis, Paris 11, 2013. (Cited on page 3.)
- [13] M. Carrière, M. Cuturi, and S. Oudot. Sliced Wasserstein kernel for persistence diagrams. In *Proceedings of the 34th International Conference on Machine Learning-Volume 70*, pages 664–673, 2017. (Cited on page 1.)
- [14] L. Chen, Z. Gan, Y. Cheng, L. Li, L. Carin, and J. Liu. Graph optimal transport for cross-domain alignment. In *International Conference on Machine Learning*, pages 1542–1553. PMLR, 2020. (Cited on page 1.)
- [15] X. Chen, Y. Yang, and Y. Li. Augmented sliced Wasserstein distances. *arXiv preprint arXiv:2006.08812*, 2020. (Cited on page 1.)
- [16] S. Claiici, A. Genevay, and J. Solomon. Wasserstein measure coresets. *arXiv preprint arXiv:1805.07412*, 2018. (Cited on page 26.)

- [17] N. Courty, R. Flamary, D. Tuia, and A. Rakotomamonjy. Optimal transport for domain adaptation. *IEEE transactions on pattern analysis and machine intelligence*, 39(9):1853–1865, 2016. (Cited on page 1.)
- [18] M. Cuturi. Sinkhorn distances: Lightspeed computation of optimal transport. In *Advances in neural information processing systems*, pages 2292–2300, 2013. (Cited on pages 1 and 3.)
- [19] A. De Acosta. Invariance principles in probability for triangular arrays of b-valued random vectors and some applications. *The Annals of Probability*, pages 346–373, 1982. (Cited on page 19.)
- [20] I. Deshpande, Y.-T. Hu, R. Sun, A. Pyrros, N. Siddiqui, S. Koyejo, Z. Zhao, D. Forsyth, and A. G. Schwing. Max-sliced Wasserstein distance and its use for GANs. In *Proceedings of the IEEE Conference on Computer Vision and Pattern Recognition*, pages 10648–10656, 2019. (Cited on page 1.)
- [21] I. Deshpande, Z. Zhang, and A. G. Schwing. Generative modeling using the sliced Wasserstein distance. In *Proceedings of the IEEE conference on computer vision and pattern recognition*, pages 3483–3491, 2018. (Cited on pages 2, 9, 30, and 31.)
- [22] V. Dobrić and J. E. Yukich. Asymptotics for transportation cost in high dimensions. *Journal of Theoretical Probability*, 8:97–118, 1995. (Cited on page 20.)
- [23] R. M. Dudley. The speed of mean Glivenko-Cantelli convergence. *Annals of Mathematical Statistics*, 40:40–50, 1969. (Cited on page 20.)
- [24] K. Fatras, Y. Zine, R. Flamary, R. Gribonval, and N. Courty. Learning with minibatch Wasserstein: asymptotic and gradient properties. In *AISTATS 2020-23rd International Conference on Artificial Intelligence and Statistics*, volume 108, pages 1–20, 2020. (Cited on pages 2, 4, 7, 10, 27, and 34.)
- [25] K. Fatras, Y. Zine, S. Majewski, R. Flamary, R. Gribonval, and N. Courty. Minibatch optimal transport distances; analysis and applications. *arXiv preprint arXiv:2101.01792*, 2021. (Cited on pages 2 and 7.)
- [26] S. Ferradans, N. Papadakis, G. Peyré, and J.-F. Aujol. Regularized discrete optimal transport. *SIAM Journal on Imaging Sciences*, 7(3):1853–1882, 2014. (Cited on pages 1 and 9.)
- [27] J. Feydy, T. Séjourné, F.-X. Vialard, S.-i. Amari, A. Trounev, and G. Peyré. Interpolating between optimal transport and mmd using Sinkhorn divergences. In *The 22nd International Conference on Artificial Intelligence and Statistics*, pages 2681–2690, 2019. (Cited on pages 12, 33, and 35.)
- [28] N. Fournier and A. Guillin. On the rate of convergence in Wasserstein distance of the empirical measure. *Probability Theory and Related Fields*, 162:707–738, 2015. (Cited on page 20.)
- [29] A. Genevay, G. Peyre, and M. Cuturi. Learning generative models with Sinkhorn divergences. In *International Conference on Artificial Intelligence and Statistics*, pages 1608–1617, 2018. (Cited on pages 1, 2, 9, 11, 30, and 31.)

- [30] I. Goodfellow, J. Pouget-Abadie, M. Mirza, B. Xu, D. Warde-Farley, S. Ozair, A. Courville, and Y. Bengio. Generative adversarial nets. In *Advances in neural information processing systems*, pages 2672–2680, 2014. (Cited on page 9.)
- [31] M. Heusel, H. Ramsauer, T. Unterthiner, B. Nessler, and S. Hochreiter. Gans trained by a two time-scale update rule converge to a local nash equilibrium. In *Advances in Neural Information Processing Systems*, pages 6626–6637, 2017. (Cited on pages 11 and 34.)
- [32] N. Ho, X. Nguyen, M. Yurochkin, H. H. Bui, V. Huynh, and D. Phung. Multilevel clustering via Wasserstein means. In *International Conference on Machine Learning*, pages 1501–1509, 2017. (Cited on page 1.)
- [33] B. Jiang. Approximate Bayesian computation with Kullback-Leibler divergence as data discrepancy. In *International Conference on Artificial Intelligence and Statistics*, pages 1711–1721, 2018. (Cited on page 26.)
- [34] E. Klinger, D. Rickert, and J. Hasenauer. pyabc: distributed, likelihood-free inference. *Bioinformatics*, 34(20):3591–3593, 2018. (Cited on page 10.)
- [35] S. Kolouri, K. Nadjahi, U. Simsekli, R. Badeau, and G. Rohde. Generalized sliced Wasserstein distances. In *Advances in Neural Information Processing Systems*, pages 261–272, 2019. (Cited on page 1.)
- [36] S. Kolouri, P. E. Pope, C. E. Martin, and G. K. Rohde. Sliced Wasserstein auto-encoders. In *International Conference on Learning Representations*, 2018. (Cited on page 2.)
- [37] A. Krizhevsky. Learning multiple layers of features from tiny images. Technical report, 2009. (Cited on page 11.)
- [38] Y. LeCun, L. Bottou, Y. Bengio, and P. Haffner. Gradient-based learning applied to document recognition. *Proceedings of the IEEE*, 86(11):2278–2324, 1998. (Cited on page 11.)
- [39] L. Li, A. Genevay, M. Yurochkin, and J. M. Solomon. Continuous regularized Wasserstein barycenters. *Advances in Neural Information Processing Systems*, 33, 2020. (Cited on page 1.)
- [40] T. Lin, C. Fan, N. Ho, M. Cuturi, and M. I. Jordan. Projection robust Wasserstein distance and Riemannian optimization. In *Advances in neural information processing systems*, 2020. (Cited on page 2.)
- [41] T. Lin, N. Ho, and M. Jordan. On efficient optimal transport: An analysis of greedy and accelerated mirror descent algorithms. In *International Conference on Machine Learning*, pages 3982–3991, 2019. (Cited on pages 1, 3, and 6.)
- [42] T. Lin, Z. Zheng, E. Y. Chen, M. Cuturi, and M. I. Jordan. On projection robust optimal transport: Sample complexity and model misspecification. *arXiv preprint arXiv:2006.12301*, 2020. (Cited on page 2.)
- [43] Z. Liu, P. Luo, X. Wang, and X. Tang. Deep learning face attributes in the wild. In *Proceedings of International Conference on Computer Vision (ICCV)*, December 2015. (Cited on page 11.)

- [44] A. Liutkus, U. Simsekli, S. Majewski, A. Durmus, and F.-R. Stöter. Sliced-Wasserstein flows: Nonparametric generative modeling via optimal transport and diffusions. In *International Conference on Machine Learning*, pages 4104–4113. PMLR, 2019. (Cited on pages 1 and 9.)
- [45] G. Mena and J. Weed. Statistical bounds for entropic optimal transport: sample complexity and the central limit theorem. In *Advances in Neural Information Processing Systems*, 2019. (Cited on page 7.)
- [46] B. Muzellec and M. Cuturi. Subspace detours: Building transport plans that are optimal on subspace projections. In *Advances in Neural Information Processing Systems*, pages 6917–6928, 2019. (Cited on page 2.)
- [47] K. Nadjahi, V. De Bortoli, A. Durmus, R. Badeau, and U. Şimşekli. Approximate Bayesian computation with the sliced-Wasserstein distance. In *ICASSP 2020-2020 IEEE International Conference on Acoustics, Speech and Signal Processing (ICASSP)*, pages 5470–5474. IEEE, 2020. (Cited on pages 1, 10, and 26.)
- [48] K. Nadjahi, A. Durmus, U. Simsekli, and R. Badeau. Asymptotic guarantees for learning generative models with the sliced-Wasserstein distance. In *Advances in Neural Information Processing Systems*, pages 250–260, 2019. (Cited on page 2.)
- [49] K. Nguyen, N. Ho, T. Pham, and H. Bui. Distributional sliced-Wasserstein and applications to generative modeling. In *International Conference on Learning Representations*, 2021. (Cited on page 1.)
- [50] K. Nguyen, S. Nguyen, N. Ho, T. Pham, and H. Bui. Improving relational regularized autoencoders with spherical sliced fused Gromov Wasserstein. In *International Conference on Learning Representations*, 2021. (Cited on page 1.)
- [51] M. Park, W. Jitkrittum, and D. Sejdinovic. K2-abc: Approximate bayesian computation with kernel embeddings. 2016. (Cited on page 26.)
- [52] F.-P. Paty and M. Cuturi. Subspace robust Wasserstein distances. In *International Conference on Machine Learning*, pages 5072–5081, 2019. (Cited on page 2.)
- [53] O. Pele and M. Werman. Fast and robust earth mover’s distance. In *ICCV*. IEEE, 2009. (Cited on page 1.)
- [54] M. Perrot, N. Courty, R. Flamary, and A. Habrard. Mapping estimation for discrete optimal transport. *Advances in Neural Information Processing Systems*, 29:4197–4205, 2016. (Cited on pages 1 and 9.)
- [55] G. Peyré. Entropic approximation of Wasserstein gradient flows. *SIAM Journal on Imaging Sciences*, 8(4):2323–2351, 2015. (Cited on page 9.)
- [56] G. Peyré, M. Cuturi, et al. Computational optimal transport: With applications to data science. *Foundations and Trends® in Machine Learning*, 11(5-6):355–607, 2019. (Cited on page 1.)
- [57] J. Rabin, S. Ferradans, and N. Papadakis. Adaptive color transfer with relaxed optimal transport. In *2014 IEEE International Conference on Image Processing (ICIP)*, pages 4852–4856. IEEE, 2014. (Cited on page 9.)

- [58] T. Salimans, H. Zhang, A. Radford, and D. Metaxas. Improving gans using optimal transport. In *International Conference on Learning Representations*, 2018. (Cited on pages 1 and 2.)
- [59] F. Santambrogio. {Euclidean, metric, and Wasserstein} gradient flows: an overview. *Bulletin of Mathematical Sciences*, 7(1):87–154, 2017. (Cited on pages 9, 11, and 12.)
- [60] M. Sommerfeld, J. Schrieber, Y. Zemel, and A. Munk. Optimal transport: Fast probabilistic approximation with exact solvers. *Journal of Machine Learning Research*, 20(105):1–23, 2019. (Cited on page 2.)
- [61] S. Tavaré, D. J. Balding, R. C. Griffiths, and P. Donnelly. Inferring coalescence times from dna sequence data. *Genetics*, 145(2):505–518, 1997. (Cited on pages 9 and 26.)
- [62] V. Titouan, N. Courty, R. Tavenard, and R. Flamary. Optimal transport for structured data with application on graphs. In *International Conference on Machine Learning*, pages 6275–6284, 2019. (Cited on page 1.)
- [63] I. Tolstikhin, O. Bousquet, S. Gelly, and B. Schoelkopf. Wasserstein auto-encoders. In *International Conference on Learning Representations*, 2018. (Cited on page 1.)
- [64] T. Toni, D. Welch, N. Strelkowa, A. Ipsen, and M. P. Stumpf. Approximate Bayesian computation scheme for parameter inference and model selection in dynamical systems. *Journal of the Royal Society Interface*, 6(31):187–202, 2009. (Cited on page 10.)
- [65] C. Villani. *Topics in optimal transportation*. Number 58. American Mathematical Soc., 2003. (Cited on page 1.)
- [66] C. Villani. *Optimal transport: old and new*, volume 338. Springer Science & Business Media, 2008. (Cited on pages 1 and 18.)
- [67] H. Xu, D. Luo, and L. Carin. Scalable Gromov-Wasserstein learning for graph partitioning and matching. In *Advances in neural information processing systems*, pages 3052–3062, 2019. (Cited on page 1.)

Supplement to “BoMb-OT: On Batch of Mini-batches Optimal Transport”

In this supplementary material, we collect several proofs and remaining materials that were deferred from the main paper. In Appendix A, we provide the proofs of the main results in the paper. We present additional materials (e.g., m-OT’s definitions, pseudo algorithms) in Appendix B. Furthermore, we provide additional results of presented experiments in the main text in Appendix C, and their corresponding settings in Appendix D.

A Proofs

In this appendix, we give detailed proofs of theorems that are stated in the main paper.

A.1 Proof of Theorem 1

We first prove that for any probability measures μ and $\nu \in \mathcal{P}_p(\Theta)$, there exists optimal transportation plan γ^* such that

$$\mathcal{D}(\mu, \nu) = \mathbb{E}_{(X^m, Y^m) \sim \gamma^*} [d(P_{X^m}, P_{Y^m})]. \quad (5)$$

From the definition of BoMb-OT, there is a sequence of transportation plans $\gamma_n \in \Pi(\mu^{\otimes m}, \nu^{\otimes m})$ such that

$$\mathbb{E}_{(X^m, Y^m) \sim \gamma_n} [d(P_{X^m}, P_{Y^m})] \rightarrow \mathcal{D}(\mu, \nu)$$

as $n \rightarrow \infty$. Since $\Pi(\mu^{\otimes m}, \nu^{\otimes m})$ is compact in the weak* topology [66], γ_n weakly converges to some $\gamma^* \in \Pi(\mu^{\otimes m}, \nu^{\otimes m})$. Since $d(P_{x^m}, P_{y^m})$ is continuous in terms of $x^m, y^m \in \mathcal{X}^m$, an application of Portmanteau theorem leads to

$$\lim_{n \rightarrow \infty} \mathbb{E}_{(X^m, Y^m) \sim \gamma_n} [d(P_{X^m}, P_{Y^m})] \geq \mathbb{E}_{(X^m, Y^m) \sim \gamma^*} [d(P_{X^m}, P_{Y^m})].$$

Putting the above results together, we obtain

$$\mathcal{D}(\mu, \nu) = \mathbb{E}_{(X^m, Y^m) \sim \gamma^*} [d(P_{X^m}, P_{Y^m})].$$

Therefore, there exists an optimal transportation plan γ^* such that equation equation 5 holds.

We now proceed to prove that BoMb-OT is a well-defined metric in the space of Borel probability measures. First, we demonstrate that $\mathcal{D}(\mu, \nu) = 0$ if and only if $\mu = \nu$. In fact, from the definition of $\mathcal{D}(\cdot, \cdot)$, if we have two probability measures μ and ν such that $\mathcal{D}(\mu, \nu) = 0$, we find that

$$\inf_{\gamma \in \Pi(\mu^{\otimes m}, \nu^{\otimes m})} \mathbb{E}_{(X^m, Y^m) \sim \gamma} [d(P_{X^m}, P_{Y^m})] = 0.$$

Since d is a metric, it implies that there exists transportation plan $\gamma^* \in \Pi(\mu^{\otimes m}, \nu^{\otimes m})$ such that $P_{X^m} = P_{Y^m}$ γ^* -almost everywhere. It demonstrates that for each x , there exists a permutation σ_x

of $\{1, \dots, m\}$ such that $x_i = y_{\sigma_x(i)}$ for all $i \in [m]$. Now, for any test function $f : \mathcal{X} \rightarrow \mathbb{R}$, we have

$$\begin{aligned} \int_{\mathcal{X}^m} \prod_{i=1}^m f(x_i) d\mu^{\otimes m}(x) &= \int_{\mathcal{X}^m \times \mathcal{X}^m} \prod_{i=1}^m f(x_i) d\gamma^*(x, y) = \int_{\mathcal{X}^m \times \mathcal{X}^m} \prod_{i=1}^m f(y_{\sigma_x(i)}) d\gamma^*(x, y) \\ &= \int_{\mathcal{X}^m \times \mathcal{X}^m} \prod_{i=1}^m f(y_i) d\gamma^*(x, y) \\ &= \int_{\mathcal{X}^m} \prod_{i=1}^m f(y_i) d\nu^{\otimes m}(y). \end{aligned}$$

Since $\int_{\mathcal{X}^m} \prod_{i=1}^m f(x_i) d\mu^{\otimes m}(x) = (\int_{\mathcal{X}} f(x_1) d\mu(x_1))^m$ and $\int_{\mathcal{X}^m} \prod_{i=1}^m f(y_i) d\nu^{\otimes m}(y) = (\int_{\mathcal{X}} f(y_1) d\nu(y_1))^m$, the above results show that

$$\int_{\mathcal{X}} f(x_1) d\mu(x_1) = \int_{\mathcal{X}} f(y_1) d\nu(y_1)$$

for any test function $f : \mathcal{X} \rightarrow \mathbb{R}$. It indicates that $\mu = \nu$. On the other hand, if $\mu = \nu$, we have $\mu^{\otimes m} = \nu^{\otimes m}$. We can construct the transportation plan $\bar{\gamma}(x, y) = \delta_x(y) \mu^{\otimes m}(x)$ for all (x, y) . Then, we find that

$$\mathcal{D}(\mu, \nu) \leq \mathbb{E}_{(X, Y) \sim \bar{\gamma}}[d(P_{X^m}, P_{Y^m})] = 0.$$

Therefore, we obtain the conclusion that $\mathcal{D}(\mu, \nu) = 0$ if and only if $\mu = \nu$.

Now, we demonstrate the triangle inequality property of $\mathcal{D}(\cdot, \cdot)$, namely, we will show that for any probability measures μ_1, μ_2 , and μ_3 , we have

$$\mathcal{D}(\mu_1, \mu_2) + \mathcal{D}(\mu_2, \mu_3) \geq \mathcal{D}(\mu_1, \mu_3).$$

The proof of this inequality is a direct application of gluing lemma [5, 19]. In particular, for any transportation plans $\gamma_1 \in \Pi(\mu_1^{\otimes m}, \mu_2^{\otimes m})$ and $\gamma_2 \in \Pi(\mu_2^{\otimes m}, \mu_3^{\otimes m})$, we can construct a probability measure ξ on $\mathcal{X}^m \times \mathcal{X}^m \times \mathcal{X}^m$ such that $\xi(\cdot, \cdot, \mathcal{X}^m) = \gamma_1(\cdot, \cdot)$ and $\xi(\mathcal{X}^m, \cdot, \cdot) = \gamma_2(\cdot, \cdot)$. Therefore, we find that

$$\begin{aligned} &\mathbb{E}_{(X, Y) \sim \gamma_1}[d(P_{X^m}, P_{Y^m})] + \mathbb{E}_{(Y, Z) \sim \gamma_2}[d(P_{Y^m}, P_{Z^m})] \\ &= \int_{(\mathcal{X}^m)^3} [d(P_{x^m}, P_{y^m}) + d(P_{y^m}, P_{z^m})] d\xi(x, y, z) \\ &\geq \int_{(\mathcal{X}^m)^3} d(P_{x^m}, P_{z^m}) d\xi(x, y, z) \geq \mathcal{D}(\mu_1, \mu_3). \end{aligned}$$

Taking the infimum on the LHS of the above inequality with respect to γ_1 and γ_2 , we obtain the triangle inequality property of $\mathcal{D}(\cdot, \cdot)$. As a consequence, we reach the conclusion of the theorem.

A.2 Proof of Theorem 2

Recall that, $d \equiv W_p$. To ease the presentation, for any product measures $\mu^{\otimes m}$ and $\nu^{\otimes m}$, we denote the following loss between $\mu^{\otimes m}$ and $\nu^{\otimes m}$ as follows:

$$\bar{\mathcal{D}}(\mu^{\otimes m}, \nu^{\otimes m}) := \inf_{\gamma \in \Pi(\mu^{\otimes m}, \nu^{\otimes m})} \mathbb{E}_{(X^m, Y^m) \sim \gamma}[d(P_{X^m}, P_{Y^m})].$$

From the definitions of (empirical) BoMb-OT losses, we have $\mathcal{D}(\mu, \nu) = \bar{\mathcal{D}}(\mu^{\otimes m}, \nu^{\otimes m})$ and $\tilde{\mathcal{D}}_k(\mu, \nu) = \bar{\mathcal{D}}(\mu_k^{\otimes m}, \nu_k^{\otimes m})$. Using the similar proof argument as that of Theorem 1, we can check that *bomb* satisfies the triangle inequality, namely, for any product measures $\mu_1^{\otimes m}, \mu_2^{\otimes m}$, and $\mu_3^{\otimes m}$, we have $\bar{\mathcal{D}}(\mu_1^{\otimes m}, \mu_2^{\otimes m}) + \bar{\mathcal{D}}(\mu_2^{\otimes m}, \mu_3^{\otimes m}) \geq \bar{\mathcal{D}}(\mu_1^{\otimes m}, \mu_3^{\otimes m})$.

From the above definition and properties of $\bar{\mathcal{D}}$, we find that

$$\begin{aligned} |\tilde{\mathcal{D}}_k(\mu, \nu) - \mathcal{D}(\mu, \nu)| &= |\bar{\mathcal{D}}(\mu_k^{\otimes m}, \nu_k^{\otimes m}) - \bar{\mathcal{D}}(\mu^{\otimes m}, \nu^{\otimes m})| \\ &\leq |\bar{\mathcal{D}}(\mu_k^{\otimes m}, \nu_k^{\otimes m}) - \bar{\mathcal{D}}(\mu^{\otimes m}, \nu_k^{\otimes m})| + |\bar{\mathcal{D}}(\mu^{\otimes m}, \nu_k^{\otimes m}) - \bar{\mathcal{D}}(\mu^{\otimes m}, \nu^{\otimes m})| \\ &\leq \bar{\mathcal{D}}(\mu_k^{\otimes m}, \mu^{\otimes m}) + \bar{\mathcal{D}}(\nu_k^{\otimes m}, \nu^{\otimes m}). \end{aligned}$$

Since $d \equiv W_p$ where $p \geq 1$, we have

$$\begin{aligned} d(P_{X^m}, P_{Y^m}) &= W_p(P_{X^m}, P_{Y^m}) = \frac{1}{m^{1/p}} \left(\inf_{\sigma} \sum_{i=1}^m \|X_i - Y_{\sigma(i)}\|^p \right)^{1/p} \\ &\leq \frac{1}{m^{1/p}} \sum_{i=1}^m \|X_i - Y_i\|, \end{aligned}$$

where the infimum is taken over all possible permutations σ of $\{1, 2, \dots, m\}$. The above inequality indicates that

$$\bar{\mathcal{D}}(\mu_k^{\otimes m}, \mu^{\otimes m}) \leq \inf_{\gamma \in \Pi(\mu_k^{\otimes m}, \mu^{\otimes m})} \mathbb{E}_{(X^m, Y^m) \sim \gamma} \left[\frac{1}{m^{1/p}} \sum_{i=1}^m \|X_i - Y_i\| \right] = m^{1-1/p} \cdot W_1(\mu_k, \mu).$$

Since \mathcal{X} is a compact subset of \mathbb{R}^N , the results of [23, 22, 28] show that $W_1(\mu_k, \mu) = \mathcal{O}_P(k^{-1/N})$. Collecting these results together, we have

$$\bar{\mathcal{D}}(\mu_k^{\otimes m}, \mu^{\otimes m}) = \mathcal{O}_P \left(\frac{m^{1-1/p}}{k^{1/N}} \right).$$

With similar argument, we also find that $\bar{\mathcal{D}}(\nu_k^{\otimes m}, \nu^{\otimes m}) = \mathcal{O}_P \left(\frac{m^{1-1/p}}{k^{1/N}} \right)$. Putting all the above results together, we reach the conclusion of the theorem.

A.3 Sample complexity of empirical BoMb-OT loss when $d \equiv SW_p$

In this section, we provide additional result with the sample complexity of empirical BoMb-OT loss when $d \equiv SW_p$.

Theorem 3. *Assume that $d \equiv SW_p$ for some $p \geq 1$ and \mathcal{X} is a compact subset of \mathbb{R}^N . Then, the following holds:*

$$|\tilde{\mathcal{D}}_k(\mu, \nu) - \mathcal{D}(\mu, \nu)| = \mathcal{O}_P \left(\frac{m^{1-1/p}}{k^{1/2}} \right).$$

The proof of Theorem 3 is direct from the proof of Theorem 2 and the results that $SW_p(\mu_k, \mu) = \mathcal{O}_P(k^{-1/2})$ and $SW_p(\nu_k, \nu) = \mathcal{O}_P(k^{-1/2})$ when \mathcal{X} is a compact subset of \mathbb{R}^N [9]. Therefore, the proof is omitted.

B Additional materials

In this appendix, we give definitions of m-OT's variants including discrete m-OT, sub-sampling m-OT and their corresponding transportation plan. We then present the pseudo code for the computation of BoMb-OT and its transportation plan. Finally, we discuss the additional computational complexities of empirical BoMb-OT loss when $d \equiv \{W_p^\tau, SW_p\}$.

B.1 Mini-batch OT

We first give definitions of discrete m-OT, sub-sampling m-OT and corresponding transportation plans. In practice, we are given $X^n := x_1, \dots, x_n$ i.i.d. samples from the distribution μ and $Y^n := y_1, \dots, y_n$ i.i.d. samples from the distribution ν where n is the given sample size. Let $\mu_n = \frac{1}{n} \sum_{i=1}^n \delta x_i$ and $\frac{1}{n} \sum_{i=1}^n \delta y_i$ be two corresponding empirical measures over previous sampled points.

Given these notations, the discrete version of m-OT loss, named *discrete m-OT*, takes the following form.

Definition 8. *The discrete m-OT loss between probability measures μ and ν is given by:*

$$U_d^n(\mu, \nu) := \frac{1}{\binom{n}{m}^2} \sum_{i=1}^{\binom{n}{m}} \sum_{j=1}^{\binom{n}{m}} d(P_{X_i^m}, P_{Y_j^m})$$

where $(X_1^m, Y_1^m), \dots, (X_{\binom{n}{m}}^m, Y_{\binom{n}{m}}^m)$ is in $\binom{X^n}{m} \times \binom{Y^n}{m}$.

Since n is often a very large number in practice, the sub-sampling version of m-OT loss is proposed. Instead of using all $\binom{n}{m}$ sets, this version only uses $k > 0$ sets of m samples.

The sub-sampling m-OT is defined as:

Definition 9. *The sub-sampling m-OT loss between probability measures μ and ν is given by:*

$$U_d^k(\mu, \nu) := \frac{1}{k^2} \sum_{i=1}^k \sum_{j=1}^k d(P_{X_i^m}, P_{Y_j^m})$$

where $(X_1^m, Y_1^m), \dots, (X_k^m, Y_k^m)$ draw uniformly from $\binom{X^n}{m} \times \binom{Y^n}{m}$.

For each $X_i^m \in \binom{X^n}{m}$ and $Y_j^m \in \binom{Y^n}{m}$, we denote by $\pi_{X_i^m, Y_j^m}$ the transportation plan between $P_{X_i^m}$ and $P_{Y_j^m}$ such that $\pi_{X_i^m, Y_j^m}$ is a $n \times n$ matrix where all entries equal zero except those indexed of samples in $X_i^m \times Y_j^m$.

Definition 10. *The m-OT's transportation matrix is defined as follows:*

$$\pi_m(\mu_n, \nu_n) := \frac{1}{\binom{n}{m}^2} \sum_{i=1}^{\binom{n}{m}} \sum_{j=1}^{\binom{n}{m}} \pi_{X_i^m, Y_j^m}. \quad (6)$$

Since $\binom{n}{m}$ is often large in practice, we also consider the subsampling version of the BoMb-OT's transportation plan:

Definition 11. Let k be a positive integer, $X_1^m, \dots, X_k^m \in \binom{X^n}{m}$ and $Y_1^m, \dots, Y_k^m \in \binom{Y^n}{m}$. The sub-sampling transportation matrix of m -OT is defined as:

$$\pi_k(\mu_n, \nu_n) := \frac{1}{k^2} \sum_{i=1}^k \sum_{j=1}^k \pi_{X_i^m, Y_j^m}. \quad (7)$$

B.2 BoMb-OT algorithm

The pseudo algorithm for computing sub-sampling BoMb-OT and its transportation plan is given in Algorithm 1.

Algorithm 1 Batch of Mini-Batches Optimal Transport

Input: $X_1^m, \dots, X_k^m \in \binom{X^n}{m}$ and $Y_1^m, \dots, Y_k^m \in \binom{Y^n}{m}$; p

$\mu_k^{\otimes m} := \frac{1}{k} \sum_{i=1}^k \delta_{X_i}$, $\nu_k^{\otimes m} := \frac{1}{k} \sum_{i=1}^k \delta_{Y_i}$

Initialize $C \in \mathbb{R}^{k \times k}$

for $i = 1$ **to** k **do**

for $j = 1$ **to** k **do**

 Compute the OT problem OT_{ij} between $P_m^{X_i} := \frac{1}{m} \sum_{i'=1}^m \delta_{X_{ii'}}$ and $P_m^{Y_j} := \frac{1}{m} \sum_{j'=1}^m \delta_{Y_{jj'}}$

$C_{ij}, \pi_{X_i, Y_j} \leftarrow OT_{ij}$

end for

end for

$\gamma \leftarrow \arg \min_{\gamma \in \Pi(\mu_k^{\otimes m}, \nu_k^{\otimes m})} \langle C, \gamma \rangle$ by LP or Sinkhorn iteration.

$\pi_k^\gamma = \sum_{i=1, j=1}^k \gamma_{i,j} \pi_{X_i, Y_j}$

Output: $\langle C, \gamma \rangle, \pi_k^\gamma$

B.3 Additional computational complexities of empirical BoMb-OT loss

We now discuss the computational complexities of empirical BoMb-OT loss when $d \equiv \{W_p^\tau, SW_p\}$. When $d \equiv W_p^\tau$ for some given regularized parameter $\tau > 0$, we can use Sinkhorn algorithm to compute $d(P_{X_i^m}, P_{Y_j^m})$ for any $1 \leq i, j \leq k$. The computational complexity of Sinkhorn algorithm for computing it is of the order $\mathcal{O}(m^2)$. Therefore, the computational complexity of computing the cost matrix from the empirical BoMb-OT is of the order $\mathcal{O}(m^2 k^2)$. Given the cost matrix, the empirical BoMb-OT loss can be approximated with the complexity of the order $\mathcal{O}(k^2/\varepsilon^2)$ where ε stands for the desired accuracy. As a consequence, the total computational complexity of computing the empirical BoMb-OT is $\mathcal{O}(m^2 k^2 + k^2/\varepsilon^2)$.

When $d \equiv SW_p$, the computational complexity for computing $d(P_{X_i^m}, P_{Y_j^m})$ is of the order $\mathcal{O}(m \log m)$ for any $1 \leq i, j \leq k$. It shows that the complexity of computing the cost matrix from the empirical BoMb-OT loss is of the order $\mathcal{O}(m(\log m)k^2)$. Given the cost matrix, the complexity of approximating the empirical BoMb-OT is at the order of $\mathcal{O}(k^2/\varepsilon^2)$. Hence, the total complexity is at the order of $\mathcal{O}(m(\log m)k^2 + k^2/\varepsilon^2)$.

C Additional Experiments

In this appendix, we provide additional experimental results that are not shown in the main paper. In Appendix C.1, we further investigate the behaviour of m-OT and (e)BoMb-OT in estimating the sub-sampling transportation plan. In Appendix C.2, more details of mini-batch ABC and additional comparative experiments are presented. After that, in Appendix C.3, we state the algorithm of color transfer and carry out more experiments with various settings in different domains of images. In Appendix C.4, we describe the applications of m-OT and BoMb-OT in the parametric generative model. We also show the comparison between m-OT and (e)BoMb-OT on CelebA, CIFAR10, and accordingly generated images. Finally, we show the experiment that uses m-OT and (e)BoMb-OT in the gradient flow application in Appendix C.5.

C.1 Transportation plans

In this appendix, we further investigate the behaviour of m-OT and (e)BoMb-OT in estimating the sub-sampling transportation plan.

Sub-sampling transportation plan: To understand the behavior of sub-sampling schemes, we plot the visualization of samples matching and transportation matrices in Figure 6 given the same setting as in Section 4.1. When the size of mini-batches equals 2 and the number of mini-batches is set to be 20 or 30, the m-OT approach produces messy OT matrices and disordered matching, meanwhile the BoMb-OT can still concentrate the mass to meaningful entries of the transportation matrix, thus, its matching is acceptable. Increasing the size of mini-batches to 8, m-OT’s performance improves significantly however its matching and its matrices are visibly still not good solutions. In contrast, BoMb-OT is able to generate nearly optimal matchings and transportation matrices.

Next, we test the m-OT and BoMb-OT in real applications in the case of extremely small number of mini-batches. When there are 8 mini-batches of size 2, the m-OT still performs poorly while the BoMb-OT creates a sparser transportation matrix which is closer to the optimal solution obtained by full-OT. Similarly, with 2 mini-batches of size 8, the BoMb-OT has only 4 wrong matchings while the number of m-OT is 10. In conclusion, BoMb-OT is the better version for mini-batching with any value of the number of mini-batches and mini-batch’s size.

Entropic transportation plan of BoMb-OT: Finally, we empirically show that the transportation plan of eBoMb-OT, when the entropic regularization is sufficiently large, reverts into m-OT’s plan. The result is given in Figure 7. When $\lambda = 10^3$, both normal version and sub-sampling version of eBoMb-OT are identical to plans of m-OT with every choice of (k, m) . However, when $\lambda = 0.1$, despite not being identical to full-OT, the plans produced by the eBoMb-OT are still close to the true optimal plan.

C.2 Approximate Bayesian Computation (ABC)

In this appendix, more details of mini-batch ABC and additional comparative experiments are presented.

Review on ABC: The central task of Bayesian inference is to estimate a distribution of parameter $\theta \in \Theta$ given n data points $\{x_i\}_{i=1}^n$ and a generative model $p(x, \theta)$. By using Bayes rule, the posterior

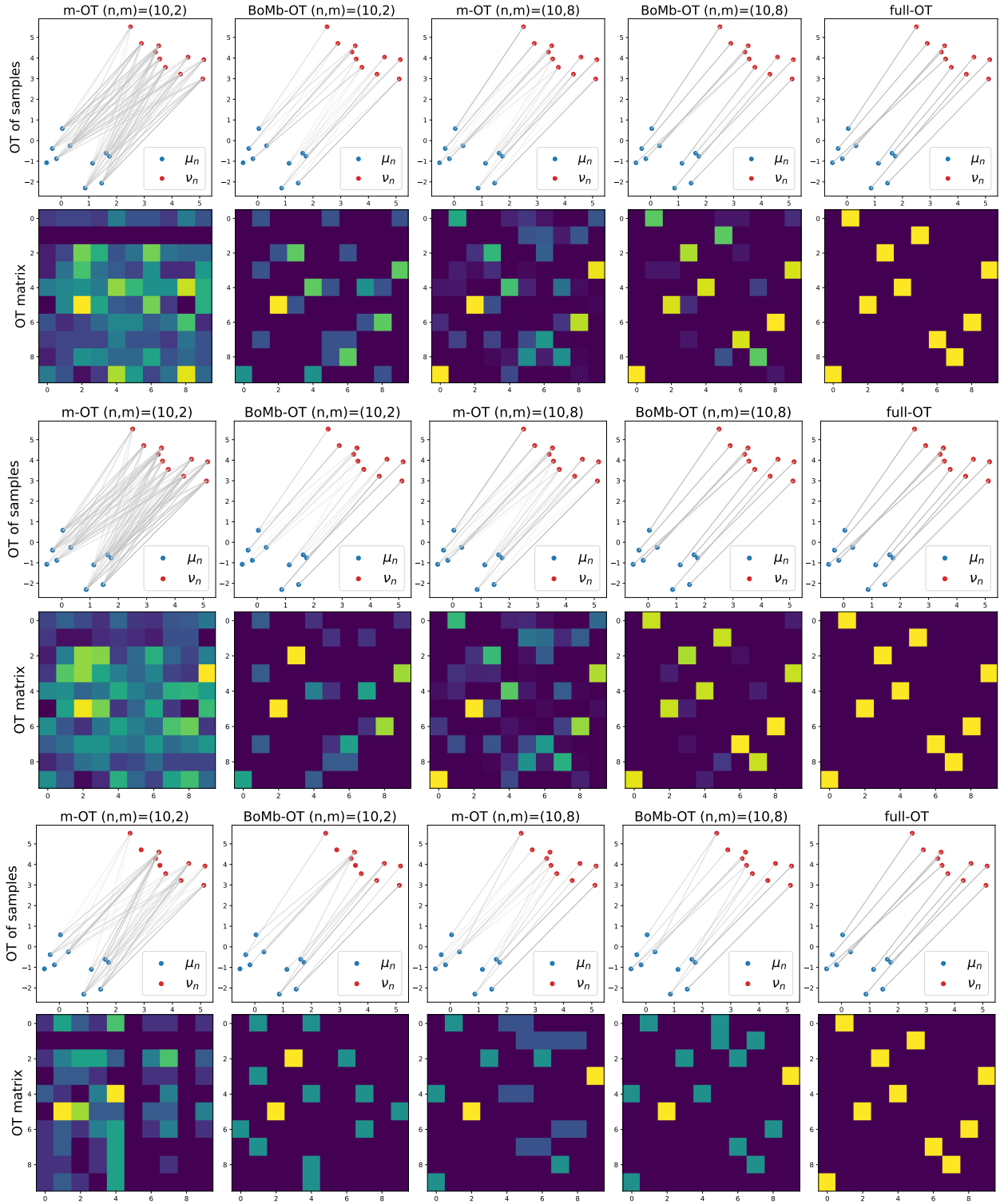


Figure 6: Visualization of sub-sampling transportation plans of m-OT and BoMb-OT between 2D empirical distributions with 10 samples. The first two rows are result of $k = 20$. The next two rows are for the $k = 30$. The last two rows are for $(k, m) = (8, 2)$ and $(k, m) = (2, 8)$ in turn.

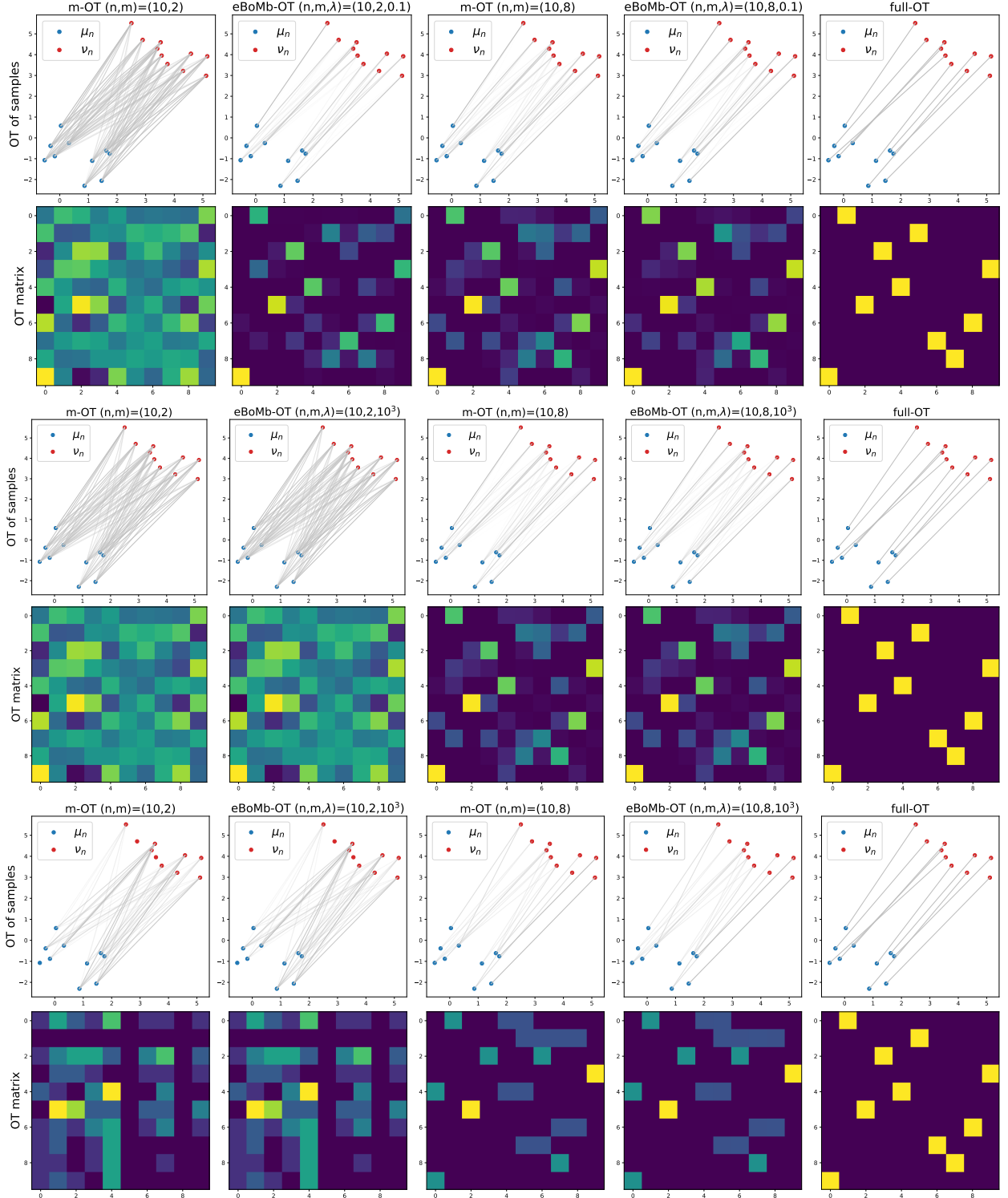


Figure 7: Visualization of eBoMb-OT's (sub-sampling) transportation plan between two 2D empirical distributions with 10 samples, and the interpolation property of eBoMb-OT. The first four rows provide the result for eBoMb-OT ($\lambda \in \{0.1, 10^3\}$), and $k \in \{2, 8\}$. The last row is the sub-sampling transportation plan with $(k, m) = (8, 2)$ and $(k, m) = (2, 8)$ respectively.

Algorithm 2 Approximate Bayesian Computation

Input: Generative model $p(x, \theta)$, observation $\{x_i\}_{i=1}^n$, number of iterations T , discrepancy measure D , tolerance threshold ϵ , number of particles m , and summary statistics s (optional).

for $t = 1$ **to** T **do**

repeat

 Sample $\theta \sim p(\theta)$

 Sample $\{y_i\}_{i=1}^m \sim p(x|\theta)$

until $D(s(\{y_i\}_{i=1}^m), s(\{x_i\}_{i=1}^n)) \leq \epsilon$

$\theta_t = \theta$

end for

Output: $\{\theta_t\}_{t=1}^T$

can be written as $p(\theta|x_{1:n}) := \frac{p(x_{1:n}|\theta)p(\theta)}{p(x_{1:n})}$. Generally, the posterior is intractable since we cannot evaluate the normalizing constant $p(x_{1:n})$ (or the evidence). It leads to the usage of approximate Bayesian Inference, e.g., Markov Chain Monte Carlo and Variational Inference. However, in some settings, the likelihood function $p(x_{1:n}|\theta)$ cannot be evaluated such as implicit generative models. In these cases, Approximate Bayesian Computation [61, 3] (or likelihood-free inference) is a good framework to infer the posterior distribution since it only requires the samples from the likelihood function.

We present a simple algorithm of ABC in Algorithm 2 that is used to obtain posterior samples of θ . The thing that sets ABC apart is that it can be implemented in distributed ways, and its posterior can be shown to have the desirable theoretical property of converging to the true posterior when $\epsilon \rightarrow 0$. However, the performance of ABC depends on the choice of the summary statistics s (e.g., empirical mean and empirical variance) and the discrepancy D . In practice, constructing sufficient statistics is not easy. Thus, a discrepancy between empirical distributions is used to avoid this non-trivial task [33, 51]. Currently, Wasserstein distances have drawn a lot of attention from ABC’s community because they provide a meaningful comparison between non-overlap probability distributions [6, 47]. In this experiment, we utilize the mini-batch Wasserstein losses as the discrepancy D to make a comparison between m-OT and BoMb-OT, and this is also the first time, to the best of our knowledge, that mini-batching OT is used in this application.

Results on mini-batch Optimal Transport ABC: In addition to the result in Figure 2 in the main paper, we plot the densities of approximated posterior in Figure 8 with several values of (k, m) . These graphs strengthen the claim that BoMb-OT outperforms m-OT in every setting of (k, m) since its posteriors are always closer to the true posterior and full-OT’s posterior than those of m-OT.

C.3 Color Transfer

In this appendix, we carry out more experiments with various settings in different domains of images.

Methodology: In our experiment, we first compress both the source image and the target image using K-means clustering with 3000 components by creating measure core-sets as in [16]. After that, we look for the transportation plans between cluster centers of two images from different approaches,

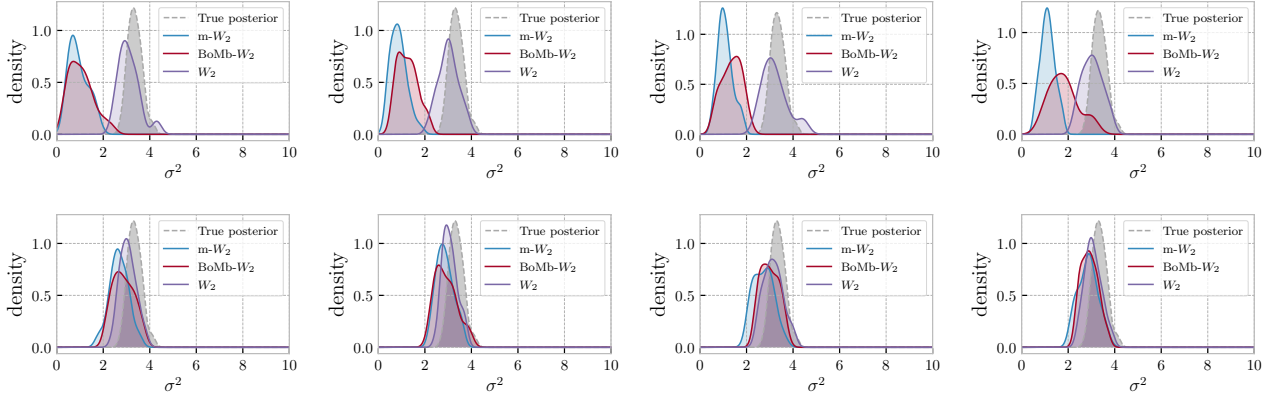


Figure 8: Approximated posteriors from ABC with different losses (m - W_2 , BoMb- W_2 , W_2), the dimension $N = 2$. For mini-batch losses ($k \in \{2, 4, 8, 16\}$), $m = 8$ in the first row and $m = 64$ in the second row.

namely m-OT, BoMb-OT, and full-OT. Next, we change the values of all pixels in a cluster of the source image based on the value of the corresponding cluster centers of the target image with the previously found plans. We present the algorithm that we use in color transfer with BoMb-OT in Algorithm 3. This algorithm is adapted from the algorithm that is used for m-OT in [24] with the key change at the estimation of the transport plan between mini-batches.

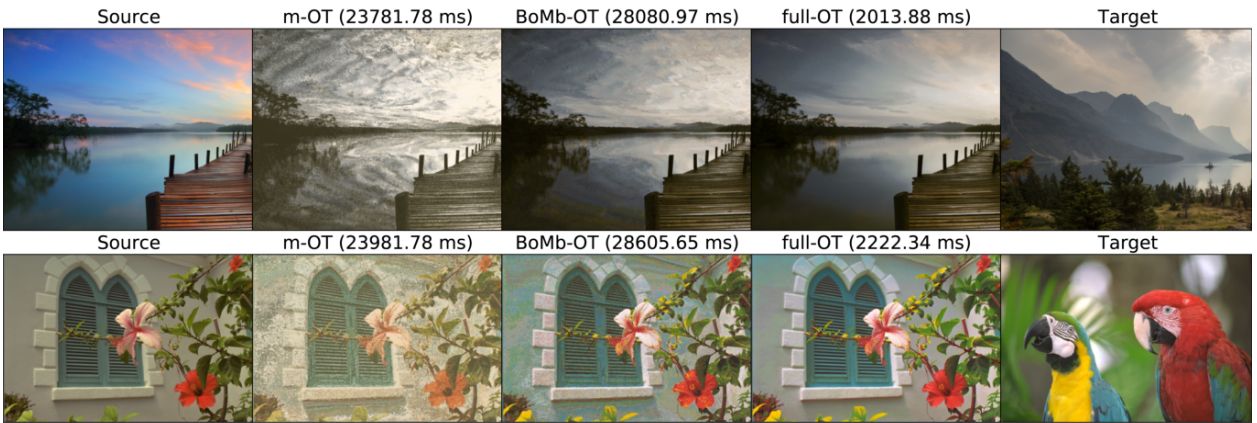
Experimental result: Next, we illustrate the color-transferred images using m-OT and BoMb-OT with several values of the number of mini-batches and the size of mini-batches (k, m) in Figure 9. It is easy to see that m-OT does not perform well when k is small, e.g. 5 or 10. Its adapted images are noisy, blurred, and are very different from the images which are obtained from the full-OT approach which are extremely smooth and natural. The performance of m-OT is only acceptable when the size of mini-batches is large enough, e.g. 60. Interestingly, the quality of BoMb-OT’s images seem to be robust to the choice of k and m . BoMb-OT’s images look similar to the full-OT’s images. Since BoMb-OT needs an additional step to compute the transport plan between mini-batches, its computational speed is always worse than m-OT. This can be seen as a trade-off between quality and speed.

Finally, to strengthen the claim on the performance of our methods on the color-transferring task, we compare BoMb-OT and m-OT on some painting images in Figure 10. This qualitative result consolidates our claim that BoMb-OT is better than m-OT in creating images with color adaptation.

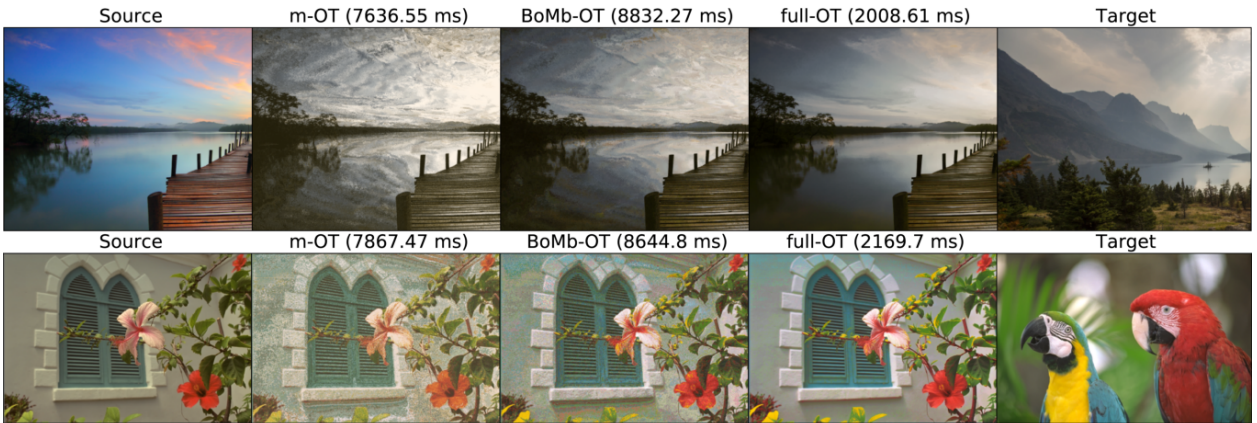
C.4 Generative model

In this appendix, we describe the applications of m-OT and BoMb-OT in the parametric generative model. We also show the comparison between m-OT and (e)BoMb-OT on CelebA, CIFAR10, and accordingly generated images.

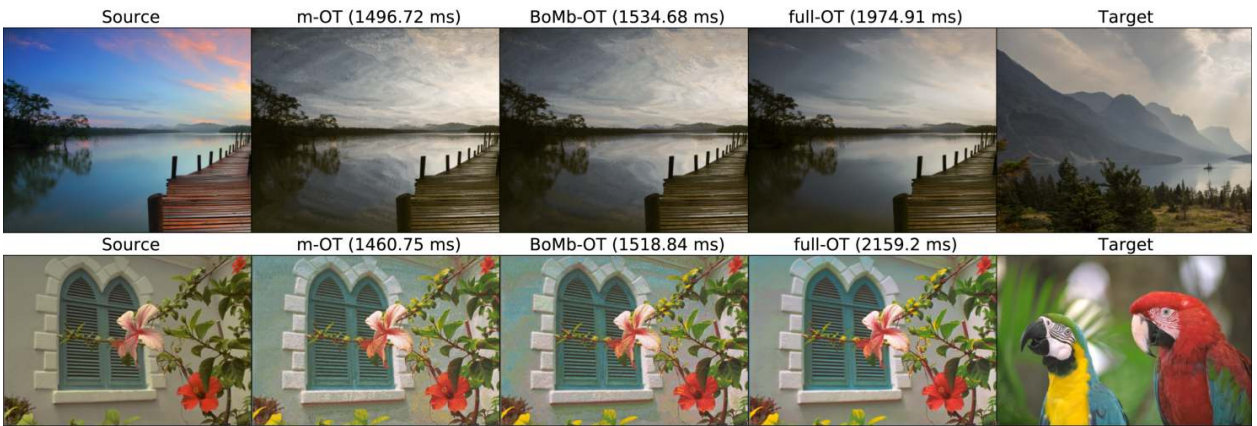
Task description: We first consider the applications of m-OT and BoMb-OT into parametric generative modeling. The ultimate goal of parametric generative modeling is to estimate a parameter of interest, says θ , which belongs to a parameter space Θ . Each value of θ induces a model distribution



Color Transfer with $k=600$ $m=5$

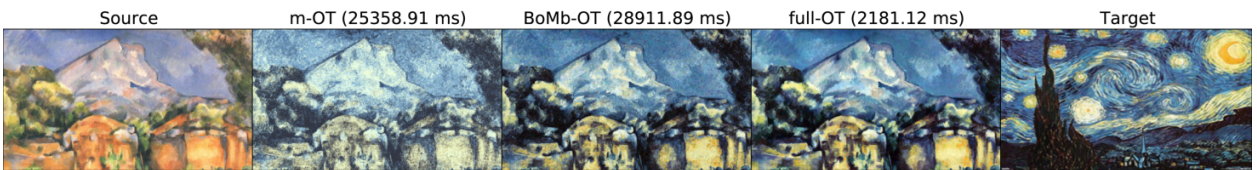


Color Transfer with $k=300$ $m=10$



Color Transfer with $k=50$ $m=60$

Figure 9: Experimental results on color transfer for m-OT, BoMb-OT for values of $(k, m) \in \{(600, 5), (300, 10), (50, 60)\}$ and corresponding computational time comparison.



Color Transfer with $k=600$ $m=5$



Color Transfer with $k=60$ $m=50$

Figure 10: Experimental results on color transfer with painting images by m-OT, BoMb-OT for $(k, m) \in \{(600, 5), (60, 50)\}$ and corresponding computational time comparison.

Algorithm 3 Color Transfer with BoMb-OT

Input: k, m , source domain $X_s \in \mathbb{R}^{n \times d}$, target domain $X_t \in \mathbb{R}^{n \times d}$
Initialize $Y_s \in \mathbb{R}^{n \times d}$
Initialize $M \in \mathbb{R}^{k \times k}$
for $i = 1$ **to** k **do**
 for $j = 1$ **to** k **do**
 Select set A_{ij} of m samples in X_s
 Select set B_{ij} of m samples in X_t
 Compute the cost matrix C_{A_i, B_j}
 $\pi_{i,j} \leftarrow \arg \min_{\pi \in \Pi(P_m^{A_{ij}}, P_m^{B_{ij}})} \langle C_{A_{ij}, B_{ij}}, \pi \rangle$
 $M_{i,j} \leftarrow \langle C_{A_{ij}, B_{ij}}, \pi_{i,j} \rangle$
 end for
end for
 $\gamma \leftarrow \arg \min_{\gamma \in \Pi(\mathcal{U}(\frac{1}{k}), \mathcal{M}(\frac{1}{k}))} \langle M, \gamma \rangle$
for $i = 1$ **to** k **do**
 for $j = 1$ **to** k **do**
 $Y_s|_{A_{ij}} \leftarrow Y_s|_{A_{ij}} + \gamma_{ij} G \cdot X_t|_{B_{ij}}$
 end for
end for
Output: Y_s

μ_θ over the data space, and we want to find the optimal parameter θ^* which has μ_{θ^*} is the closest to the empirical data distribution ν under a discrepancy (e.g. Wasserstein distance). In deep learning setting, θ is the weight of a deep neural network that map from a low dimensional manifold Z to the data space X , and the model distribution μ_θ is a push-forward distribution $\theta\#\Lambda$ for Λ is a white noise distribution on Z (e.g. $\mathcal{N}(0, I)$). By using mini-batching schemes, we can estimate this parameter by minimizing the corresponding mini-batch loss U_d :

$$\theta^* \leftarrow \arg \min_{\theta \in \Theta} U_d(\mu_\theta, \nu), \quad (8)$$

where U_d could be the m-OT loss in Definition 9, or the BoMb-OT loss in Definition 3. This optimization is used directly in learning generative model on MNIST dataset with $d \equiv (SW_2, W_2^T)$. [29, 21]

Metric learning: Since L_2 distance is not a natural distance on the space of images, metric learning was introduced by [29, 21] as a key step in the application of generative models. The general idea is to learn a parametric ground metric cost c_ϕ :

$$c_\phi(x, y) = \|f_\phi(x) - f_\phi(y)\|_2, \quad (9)$$

where $f_\phi : \mathcal{X} \rightarrow \mathbb{R}^h$ is a non-linear function that map from the data space to a feature space where L_2 distance is meaningful.

The methodology to learn the function f_ϕ depends on the choice of d . For example, when $d = W_2^T$,

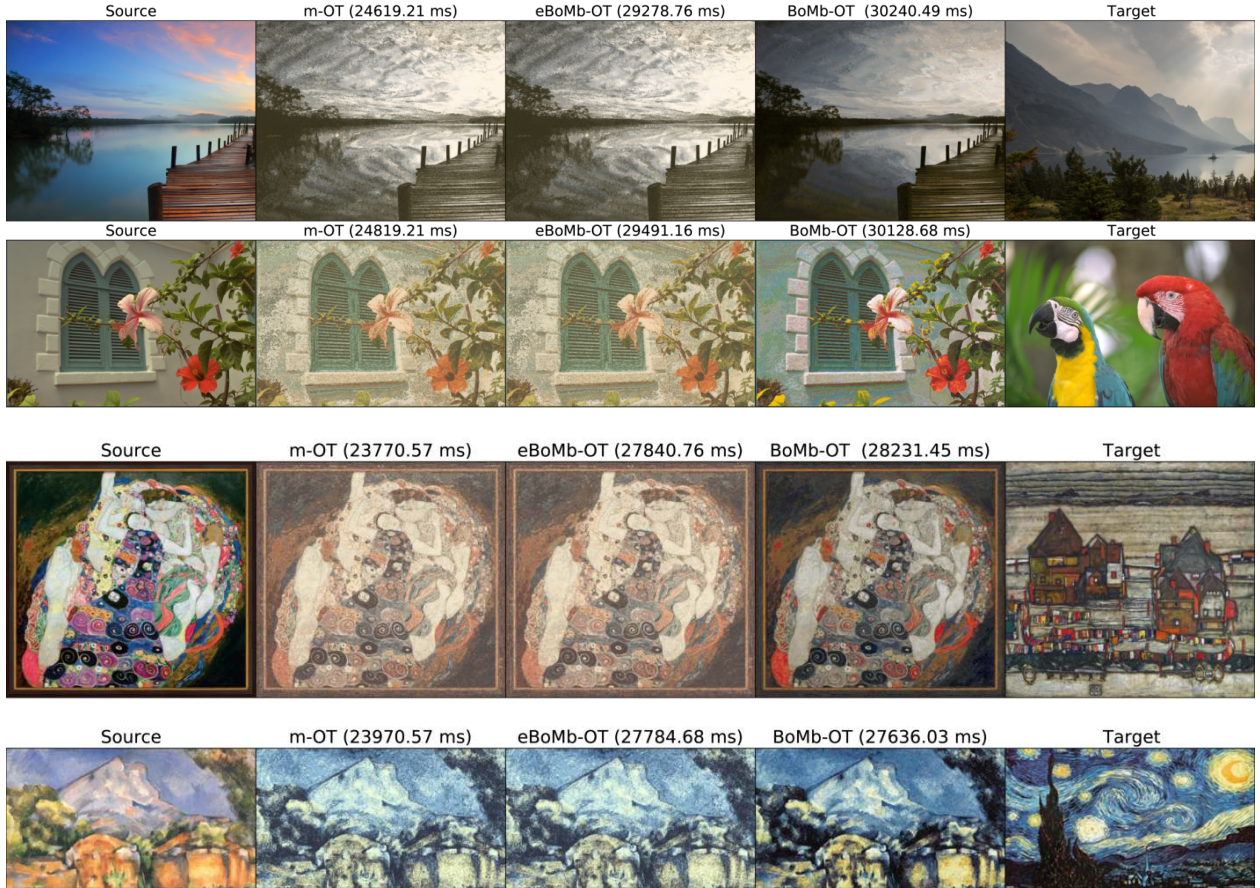


Figure 11: Visualization of interpolation property of eBoMb-OT on color transfer with $(\lambda = 10^9)$, $(k, m) = (600, 5)$, and computational time.

authors in [29] seek for ϕ by solve following optimization:

$$\max_{\phi} W_{c_{\phi}}^{\tau}(\mu_{\theta}, \nu). \quad (10)$$

In [21], another metric learning technique is used for $d = SW_2$:

$$\max_{\phi} \max_{\psi} \mathbb{E}_{X \sim \mu_{\theta}, Y \sim \nu} [\log g_{\psi}(f_{\phi}(Y)) + \log(1 - g_{\psi}(f_{\phi}(X)))], \quad (11)$$

where $g_{\psi} : \mathbb{R}^h \rightarrow [0, 1]$.

Learning the metric or f_{ϕ} is carried out simultaneously with learning the generative model in practice, namely, after one gradient step for the parameter θ , ϕ will be updated by one gradient step.

Results on CelebA and CIFAR10: It is well-known that adversarial training is unstable, thus, the obtained result cannot be well-interpreted. According to Figures 12 and 13, it is not clear

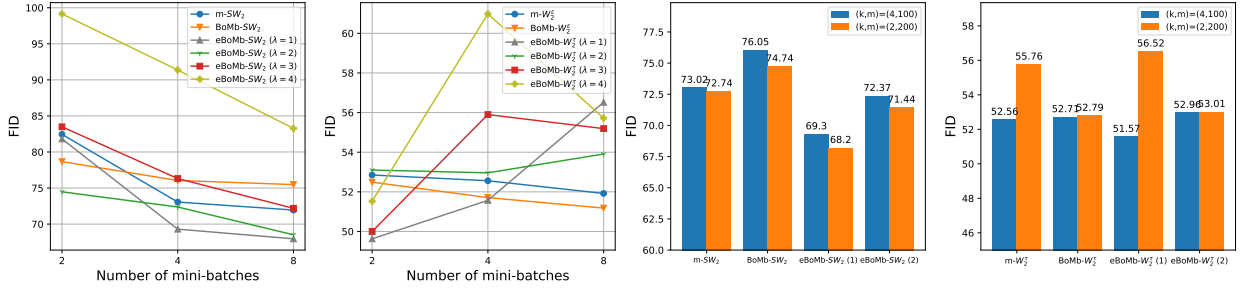


Figure 12: Comparison between BoMb-OT and m-OT on CelebA dataset with various values of k . The first two graphs show the changing of the FID score of mini-batch losses ($d \in \{SW_2, W_2^T\}$) when increasing the number of mini-batches ($k \in \{2, 4, 8\}$) on CelebA dataset. The last two graphs is comparing two settings of (k, m) which are $\{(4, 100), (2, 200)\}$.

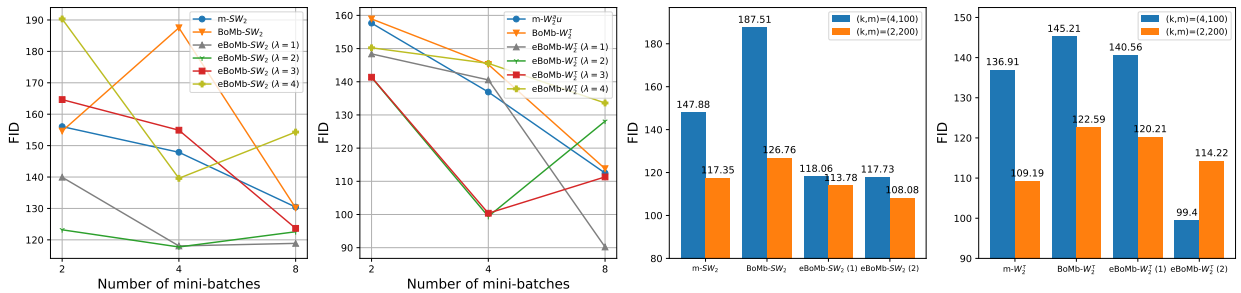


Figure 13: Comparison between BoMb-OT and m-OT on CIFAR10 dataset with various values of k . The first two graphs show the changing of the FID score of mini-batch losses ($d \in \{SW_2, W_2^T\}$) when increasing the number of mini-batches ($k \in \{2, 4, 8\}$) on CIFAR dataset. The last two graphs is comparing two settings of (k, m) which are $\{(4, 100), (2, 200)\}$.

whether increasing the number of mini-batches can improve the quality of the generative models, namely, the FID curves on CelebA and CIFAR fluctuate over the number of mini-batches. However, the best generative model is always either BoMb-OT or eBoMb-OT, since they have the lowest FID score.

Generated images: We show the generated images on MNIST dataset in Figure 14, generated images on CelebA and CIFAR10 in Figures 15 and 16, respectively. According to these images, we can see that (e)BoMb-OT is more realistic than m-OT or at least comparable.

C.5 Gradient Flow

In this appendix, we show the experiment that uses m-OT and (e)BoMb-OT in the gradient flow application.

Task description: Gradient flow is a non-parametric method to learn a generative model. Like every generative model, the goal of gradient flow is to mimic the data distribution ν by a distribution

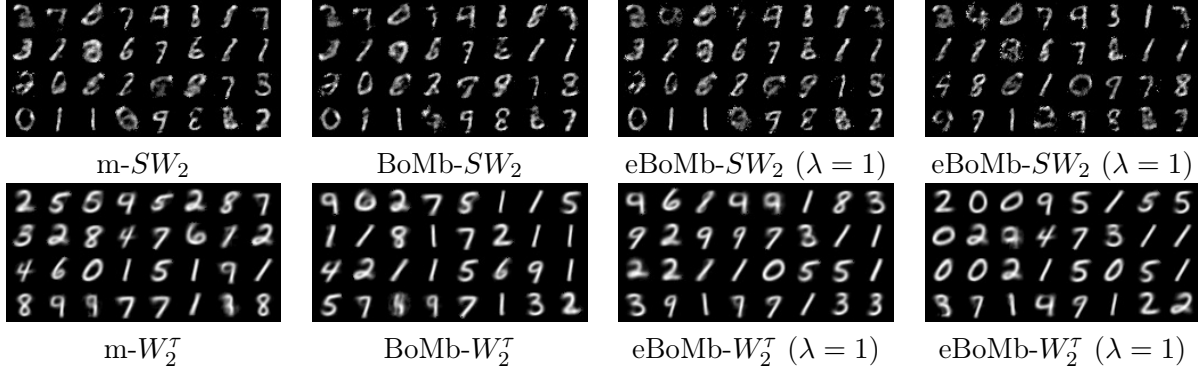


Figure 14: MNIST generated images from different mini-batch losses, $(k,m)=(4,100)$ for the first three columns, $(k,m)=(2,200)$ for the last column.

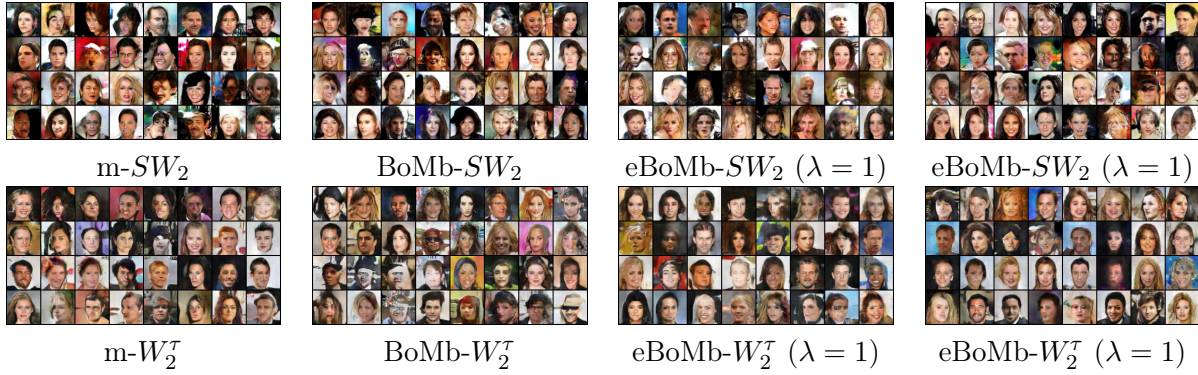


Figure 15: CelebA generated images from different mini-batch losses, $(k,m)=(4,100)$ for the first three columns, $(k,m)=(2,200)$ for the last column.

μ . It leads to the functional optimization problem:

$$\min_{\mu} D(\mu, \nu), \quad (12)$$

where D is a predefined discrepancy between two probability measures. So, a gradient flows can be constructed:

$$\partial_t \mu_t = -\nabla_{\mu_t} D(\mu_t, \nu) \quad (13)$$

We follow the Euler scheme to solve this equation as in [27], starting from an initial distribution at time $t = 0$. In this paper, we choose D be (e)BoMb- W_2 and m- W_2 for the sake of comparison between them.

Synthetic example: In addition to the experiment in the main paper, we do an extra setup with a higher size of mini-batches, $(k, m) = (50, 10)$. The result is shown in Figure 17. In this setting, BoMb-OT shows its favorable performance compared to m-OT, namely, its Wasserstein-2 scores are lower than m-OT in every step. The entropic version of BoMb-OT, eBoMb-OT, also performs better than m-OT in this setup.

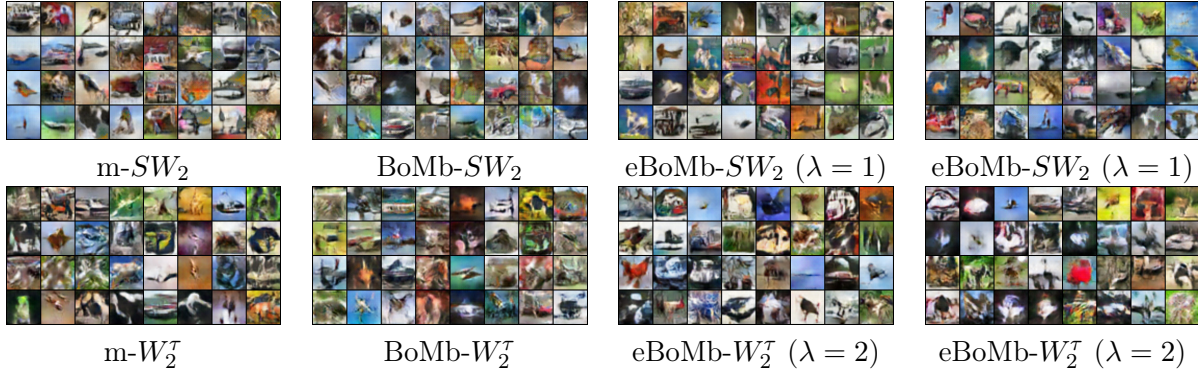


Figure 16: CIFAR10 generated images from different mini-batch losses, $(k,m)=(4,100)$ for the first three columns, $(k,m)=(2,200)$ for the last column.

CelebA: We define μ and ν are the empirical measures defined over 5000 female images and 5000 male images in the CelebA dataset, thus, We can present the transformation from male face to be a female one by creating a flow from μ to ν . Our setting experiment is the same as [24]. We first train an autoencoder on CelebA, then we compress two original measures to the low-dimensional measures on the latent space of the autoencoder. After having the latent measures, we run the Euler scheme to get the transformed measure then we decode it back to the data space by the autoencoder. The result is shown in Figure 18, we also show the closest female image (in sense of L_2 distance) to the final found image in each method and the corresponding L_2 distance between the middle step images and the nearest image. As shown, (e)BoMb-OT provides a better flow than m-OT.

D Experiment Settings

In this appendix, we collect some necessary experimental setups in the paper including generative model, gradient flow.

D.1 Parametric generative model

Wasserstein-2 scores: We use empirical distribution with 10000 samples that are obtained by sampling from the generative model and the empirical test set distribution respectively, then we compute discrete Wasserstein-2 distance via linear programming.

FID scores: We use 10000 samples from the generative model and all test set images to compute FID score by the official code from authors in [31].

Parameter settings: We chose learning rate equal to 0.0005, batch size equal to 100, number of epochs in MNIST equal to 100, number of epochs in CelebA equal to 25, and the number of epoch in CIFAR10 equal to 50. When increasing the batch size to 200, we double the number of epochs for having the same number of gradient steps. For $d = SW_2$ we use the number of projections $L = 1000$ on MNIST and $L = 100$ on CelebA and CIFAR10, respectively. For $d = W_2^\tau$, we use $\tau = 0.5$ for MNIST, $\tau = 40$ for CelebA and $\tau = 50$ for CIFAR10, the number of Sinkhorn iterations is 10.

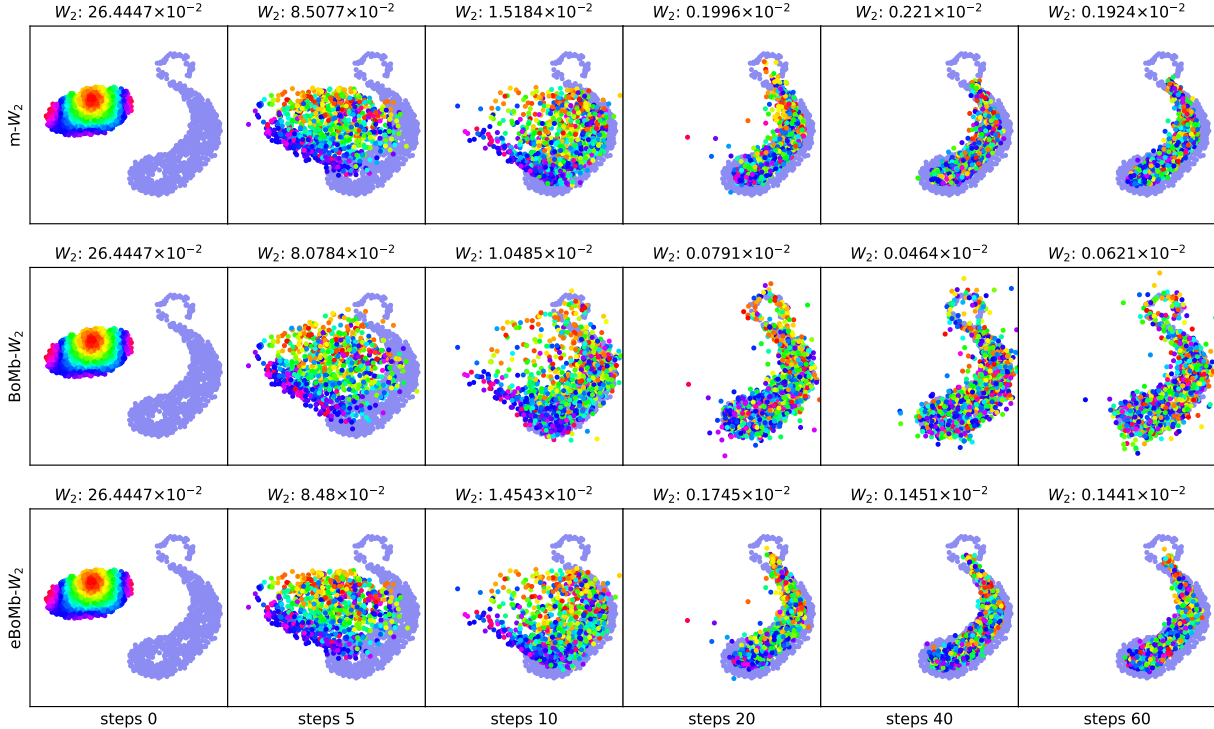


Figure 17: Visualization of the gradient flow provided by m-OT, BoMb-OT and eBoMb-OT with corresponding Wasserstein-2 scores ($n = 1000, (k, m) = (50, 10)$).

Neural network architectures: Generator architecture was used for MNIST dataset:
 $z \in \mathbb{R}^{32} \rightarrow FC_{100} \rightarrow ReLU \rightarrow FC_{200} \rightarrow ReLU \rightarrow FC_{400} \rightarrow ReLU \rightarrow FC_{784} \rightarrow ReLU$

Generator architecture was used for CelebA and CIFAR10 : $z \in \mathbb{R}^{128} \rightarrow TransposeConv_{512} \rightarrow BatchNorm \rightarrow ReLU \rightarrow TransposeConv_{256} \rightarrow BatchNorm \rightarrow ReLU \rightarrow TransposeConv_{128} \rightarrow BatchNorm \rightarrow ReLU \rightarrow TransposeConv_{64} \rightarrow BatchNorm \rightarrow ReLU \rightarrow TransposeConv_1 \rightarrow Tanh$

Metric learning neural network’s architecture was used for CelebA, CIFAR10:

First part: $x \in \mathbb{R}^{64 \times 64 \times 3} \rightarrow Conv_{64} \rightarrow LeakyReLU_{0.2} \rightarrow Conv_{128} \rightarrow BatchNorm \rightarrow LeakyReLU_{0.2} \rightarrow Conv_{256} \rightarrow BatchNorm \rightarrow LeakyReLU_{0.2} \rightarrow Conv_{512} \rightarrow BatchNorm \rightarrow Tanh$

Second part: $Conv_1 \rightarrow Sigmoid$

D.2 Gradient flow

For the implementation of the gradient flow we use the geomloss library [27]. For the autoencoder in CelebA experiments, we use the repo in https://github.com/rasbt/deeplearning-models/blob/master/pytorch_ipynb/autoencoder/ae-conv-nneighbor-celeba.ipynb for the pretrained autoencoder.

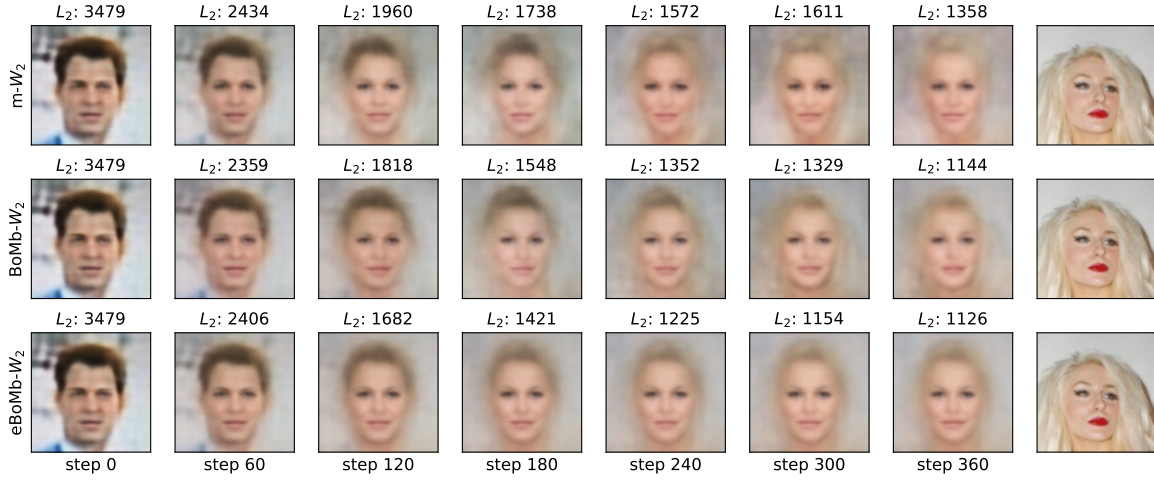


Figure 18: Transforming man face to woman face by using the gradient flow with m-OT and (e)BoMb-OT on CelebA dataset for $(k, m) = (25, 100)$. The last column is the nearest image (in sense of L_2 distance) to the final found female image, the corresponding L_2 distance are also shown on the top of middle-stage images.

D.3 Computational infrastructure

All deep learning experiments are done on GPU Tesla V100. Other experiments are done on a laptop Asus ROG Zephyrus GX550.